The life cycle of large igneous provinces

Benjamin A. Black[1,2]✉, *Leif Karlstrom*[3] *and Tamsin A. Mather*[4]

Abstract | Extremely voluminous magmatic systems known as large igneous provinces (LIPs) punctuate Earth's history, and the gases they release plausibly link large-scale geodynamic and magmatic processes with major climate shifts in Earth's geological record. However, quantifying the relationships between magmatism, gas release and environmental changes remains challenging. In this Review, we explore the major insights and outstanding questions regarding the linked evolution of mantle melting, expansive magmatic systems and the redistribution of volatiles from the solid Earth to the atmosphere. The evolution of mantle melt generation during LIP episodes sets the fundamental tempo of magma emplacement throughout the crust. The progression of crustal LIP magmatism and associated hydrothermal activity help shape the chemical evolution of the continental lithosphere and surface environment. Percolation of magmatic and metamorphic volatiles can decouple the tempo of gas release — a potential key driver of environmental changes — from the tempo of extrusive volcanic activity. LIPs demonstrate how large-scale magmatic systems interact with the surrounding lithosphere to propel evolving regimes of magma and volatile transfer through the crust. New, temporally resolved constraints on the evolution of LIP plumbing systems are needed to keep pace with increasingly precise timelines of palaeoenvironmental change during LIP emplacement.

Mass extinctions
Abrupt losses of biodiversity in which >75% of species vanish over geologically short intervals, yielding extinction rates that far exceed rates at which new species evolve.

[1]*Department of Earth and Planetary Science, Rutgers University, New Brunswick, NJ, USA.*
[2]*Department of Earth and Atmospheric Science, CUNY City College, New York, NY, USA.*
[3]*Department of Earth Sciences, University of Oregon, Eugene, OR, USA.*
[4]*Department of Earth Sciences, University of Oxford, Oxford, UK.*
✉*e-mail: bblack@eps.rutgers.edu*

https://doi.org/10.1038/s43017-021-00221-4

Large igneous provinces (LIPs) are among the most extensive magmatic events punctuating Earth's history. They typically emplace 10^5–10^7 km^3 of mainly mafic magma on the Earth's surface and throughout the lithosphere. More than 24 oceanic and continental LIP events have occurred over the past 275 Myr (REFS[1,2]), at intervals of ~10–50 Myr (REFS[1,3,4]). Prominent examples include the ~16-Ma Columbia River Basalts (CRB), the ~66-Ma Deccan Traps, the ~110-Ma Ontong Java Plateau (OJP) and the ~252-Ma Siberian Traps. Advances in geochronology, new geochemical tools and advances in modelling of magmatic processes have opened the door to a fresh understanding of LIP magmatism and volatiles as dynamic and temporally evolving systems. Understanding the origins, evolution and consequences of LIPs are critical to reconstructing past interactions between solid Earth reservoirs and surface environments.

In the geological record, at least four of the 'big five' severest mass extinctions overlap in time with LIP events[5–9]. Many other LIPs are temporally associated with major carbon cycle perturbations and/or ocean anoxia events that drive more minor species overturn, (for example, less severe than the so-called 'big five')[5–9]. Volatile release — especially of CO_2, sulfur species and halogens — represents a potentially key causal mechanism linking LIP emplacement and major environmental changes. The large scale of LIPs, their intra-plate location and presumed deep mantle source enable them to remobilize volatiles from the deep mantle, the stable continental lithospheric mantle (CLM) and the crust[10,11].

A dynamic network of channels and storage zones links regions of LIP melt generation in the mantle with regions of magma solidification in the crust and eruption at the surface (FIG. 1), forming a transcrustal transport system[12]. These magma transport systems are exposed today as relic LIP dikes, sills and layered intrusions, including the most extensive mafic plutonic structures on Earth[13]. Vast radiating and circumferential dike swarms in Precambrian exposures, such as the 1,270-Ma Mackenzie LIP in Canada that spans >10^7 km^2, reflect the scale of crustal magma transfer[14,15]. The variety of LIP magma geochemistries, including tholeiitic and alkaline compositions, reflects the diversity of mantle melting conditions and transport pathways.

Continued advances in understanding the timing and extent of LIP volcanism have strengthened the temporal link with surface environmental changes. However, the precise mechanistic relationships between LIP activity and the progression of environmental change remain elusive. Resolving these relationships depends on

Key points

- Large igneous provinces (LIPs) mobilize climate-impacting gases from the solid Earth and have been implicated in major environmental disruptions.
- Mantle melting varies between LIPs: continental LIP main-phase melting tends to be shallower than early and late phases, whereas oceanic LIPs differ, suggesting that lithosphere thickness is among the controls modulating melting.
- LIPs exhibit an evolving lithospheric transport system that links waxing and waning generation of a prodigious volume (10^6–10^7 km^3) of mantle melt with intrusions and surface outpourings of lava.
- LIP volatiles originate from the mantle, continental lithospheric mantle and crust. Evolving magmatic chemistry, intrusion, volatile flushing and cryptic degassing complicate the relationship between pace of emissions (particularly CO_2) and surface eruption rates.
- Understanding links between LIP melt generation, lithospheric magma plumbing and surface climate requires high-resolution timelines for these systems combining geodynamic modelling, geochronology and geochemical datasets.

developing an integrated picture of evolving processes within the LIP magma transport network, with such understanding just beginning to emerge (FIG. 1).

In this Review, we discuss the life cycle of LIPs, spanning their origin, evolution and termination. Other reviews have focused on LIP surface extrusions or the link with mass extinctions[2,6–8,16,17]. Here, we address the petrology and lithospheric plumbing of LIPs, including magma storage, transport and crustal rheology. In particular, we examine how these LIP processes facilitate volatile exchange between solid Earth and surface environments. We present a compilation of volatile inventories through LIP evolution (Supplementary data) to capture emerging constraints on the scale of outgassing and variability amongst LIPs. We highlight future research directions that integrate petrologic, geochemical and geophysical techniques to resolve the architecture, timescales and consequences of LIP magmatism.

The origins of LIP magmatism

In this section, the bottom-up mantle controls on the origin and evolution of LIP magmatic systems are discussed. Variability in mantle source characteristics drives evolving LIP magma supply, volatiles and compositional evolution. Top-down processes, such as lithospheric thickening, extension or delamination, influence mantle melting and create feedbacks between mantle and lithospheric evolution.

Connections to the deep mantle. The origins of prodigious mantle melting during LIP emplacement are the subject of long-standing debate[18,19]. The plume head and tail model postulates that hot, buoyant mantle plumes maybe rooted as deep as the core–mantle boundary cause LIPs soon after plume heads first arrive at the base of the lithosphere[18,20,21]. Alternative models include edge-driven convection[20], delamination[22], impact-induced melting[23] and thermal anomalies due to changes in mantle flow or reduced mantle heat loss beneath continents[24,25].

These melting mechanisms are not mutually exclusive, and different LIPs could exhibit combinations of processes. However, seismic[26,27], geochemical[28,29] and petrologic[30–32] evidence are consistent with the view that thermochemically distinct mantle plumes exist, that some plumes begin near the core–mantle boundary[26,33,34] and that their arrival at the base of the lithosphere can initiate LIP melting[20,35]. Mantle plumes have been proposed to incorporate recycled oceanic crust[36], less degassed primordial reservoirs in the lower mantle[28,29] and perhaps even material from the core[37].

Mantle potential temperatures. Mantle potential temperatures 100–250 °C above the ambient mantle are a key factor in time-evolving LIP mantle melting. Elevated mantle potential temperatures have been inferred for LIPs, including the Siberian Traps, Caribbean LIP, Paraná-Etendeka and Deccan Traps[30–32,38], with more subtly elevated temperatures in the Central Atlantic Magmatic Province (CAMP)[31]. Higher mantle temperatures are consistent with upwelling thermochemical mantle plumes, though alternative mechanisms such as thermal insulation beneath supercontinents have also been proposed[24]. Regardless, anomalously hot mantle likely plays an important role in generating the tremendous volumes of mantle melt that characterize LIPs. Geodynamic modelling of mantle plumes implies lateral and vertical temperature gradients within the plume head, with a hot core and cooler margins[39], in line with the range in petrologically determined mantle temperatures across different magma suites[40]. Such temperature as well as pressure variations relative to the mantle solidus translate into variations in the degree of melting and volume of melt production.

Mantle temperatures likely evolve through time. Along with compositional and melting depth heterogeneity, the resulting changes in LIP melting and the volumes of melt generation help drive bottom-up shifts in the phase of the LIP life cycle. Mantle potential temperatures beneath ocean island basalts are typically 100–200 °C cooler than those beneath LIPs, pointing to broad secular cooling of mantle plumes on 10^7-year timescales[31] — possibly linked to the transition from plume heads to tails[20]. However, geothermometry from 60 Ma to the present from the North Atlantic tracks notable fluctuations in the Iceland plume[41], suggesting that increasing spatial and temporal resolution could reveal more complicated patterns of temperature evolution here and elsewhere.

Composition of mantle sources. The range of major element and trace element compositions in LIP magmas is inconsistent with a single mantle source composition. Instead, primary melts likely reflect varying proportions of recycled and enriched material from the deep mantle, shallow asthenospheric mantle similar to the source of mid-ocean ridge basalts, CLM and, in some cases, interactions with a downgoing subducting slab[36,42–44]. Trace element ratios can potentially distinguish between sources of LIP melting[45]. Mantle plume heterogeneity is recorded in the geochemistry of hotspot[46] and primitive LIP magmas[47]. However, magma storage and transport can homogenize trace element and isotope systematics, especially in main-phase basalts[48], making source heterogeneity harder to distinguish.

Subducted oceanic lithosphere is rich in volatiles relative to the average mantle[36,49]. Therefore, melting of

Continental lithospheric mantle
(CLM). The uppermost part of the mantle that is mechanically attached to continental crust and does not participate in mantle convection.

Transcrustal transport system
The suite of processes by which magma ascends through the crust to the surface via a network of storage zones (magma chambers) and dikes and/or sills.

Tholeiitic
Iron-rich basalts like those found at mid-ocean ridges, commonly thought to originate at relatively high (>10%) degrees of melting, typically at pressures <3 GPa.

Alkaline
Basalts rich in K and Na, and are thought to originate at relatively low degrees of melting (<5%), often at pressures >3 GPa.

Mantle melting
Occurs when the decompression, temperature or composition of mantle material (or a combination of these) place it above its solidus — but almost universally below its liquidus, when it would be entirely molten.

Mantle plumes
Focused upwellings from the deep mantle with anomalous composition and temperature that cause them to be buoyant.

Edge-driven convection
Invokes lithospheric thickness variations, for example, across the edges of continents, to drive local convection and decompression melting.

Delamination
When the formation of dense eclogites causes the lowermost crust or lithospheric mantle to sink into the underlying mantle.

Mantle potential temperatures
The temperatures of a parcel of mantle if brought adiabatically to the Earth's surface, which enables comparison of mantle temperatures from different depths.

Geodynamic modelling
Solves conservation equations for mass, momentum and energy to predict how the solid Earth evolves, typically focused on large length scales and timescales, and typically involving mantle convection.

Major element
An element with concentration exceeding ~1 wt% — in this case, within magmas — including Si, Fe, O, Mg, Ca and Al.

subduction-derived, recycled, pyroxenite-rich mantle could occur at higher pressures and deliver higher volatile concentrations than average mantle melting[36,50,51]. However, whether mantle plumes do entrain some recycled pyroxenite derived from subducted oceanic crust remains debated. Furthermore, the extent to which subducted volatiles such as carbon and sulfur remain coupled during recycling is a major outstanding question, owing to complicated redox transitions between the upper and lower mantle[52]. Mass-independent fractionation of sulfur isotopes has been used to detect recycled Archaean sulfur[53] and Mg isotopes have been used to detect recycled carbonates[54] in the sources of ocean island basalts, implying that some sulfur and carbon do indeed remain coupled to recycled lithologies on billion-year timescales.

Melting depths and feedbacks with the lithosphere. Constraints on melting pressures come from trace element distributions sensitive to the degree of partial melting of the mantle and presence of garnet (implying melting pressures ≥3 GPa)[36,55–58]. These models leverage experimental data for melt compositions in equilibrium with mantle minerals[59]. Melting pressure estimates for continental LIPs — including the Siberian Traps, Paraná-Etendeka and the North Atlantic Igneous Province (NAIP)[36,55–57] — are consistent with deep melting in the garnet stability field during the early and waning phases of LIPs (FIG. 2), including some alkaline and ultramafic magmas that originate from depths as great as ~6–8 GPa (~180–240 km)[56,57,60]. By contrast, during the main phase of continental LIPs, melting shallows into the spinel stability field and main-phase tholeiitic lavas from oceanic and continental LIPs originate at relatively shallow pressures of 1.5–4 GPa (~45–120 km)[56,58,61].

Leading explanations for a progression from deeper to shallower LIP melting involve thinning of the CLM through extension facilitated by thermal weakening of the lithosphere or delamination of dense pyroxene-garnet intrusions at the base of the lithosphere[22,36,62]. Decreasing melting depth through the course of continental LIP magmatism implies disruption of the CLM. Alkaline, sometimes ultrapotassic, dikes and lavas originating from low-degree (1–3%) melting of the CLM[56,63,64] are one by-product of this lithosphere disruption (FIG. 1).

Evolution from deep to shallow melting is not evident in oceanic LIPs, possibly owing to the absence

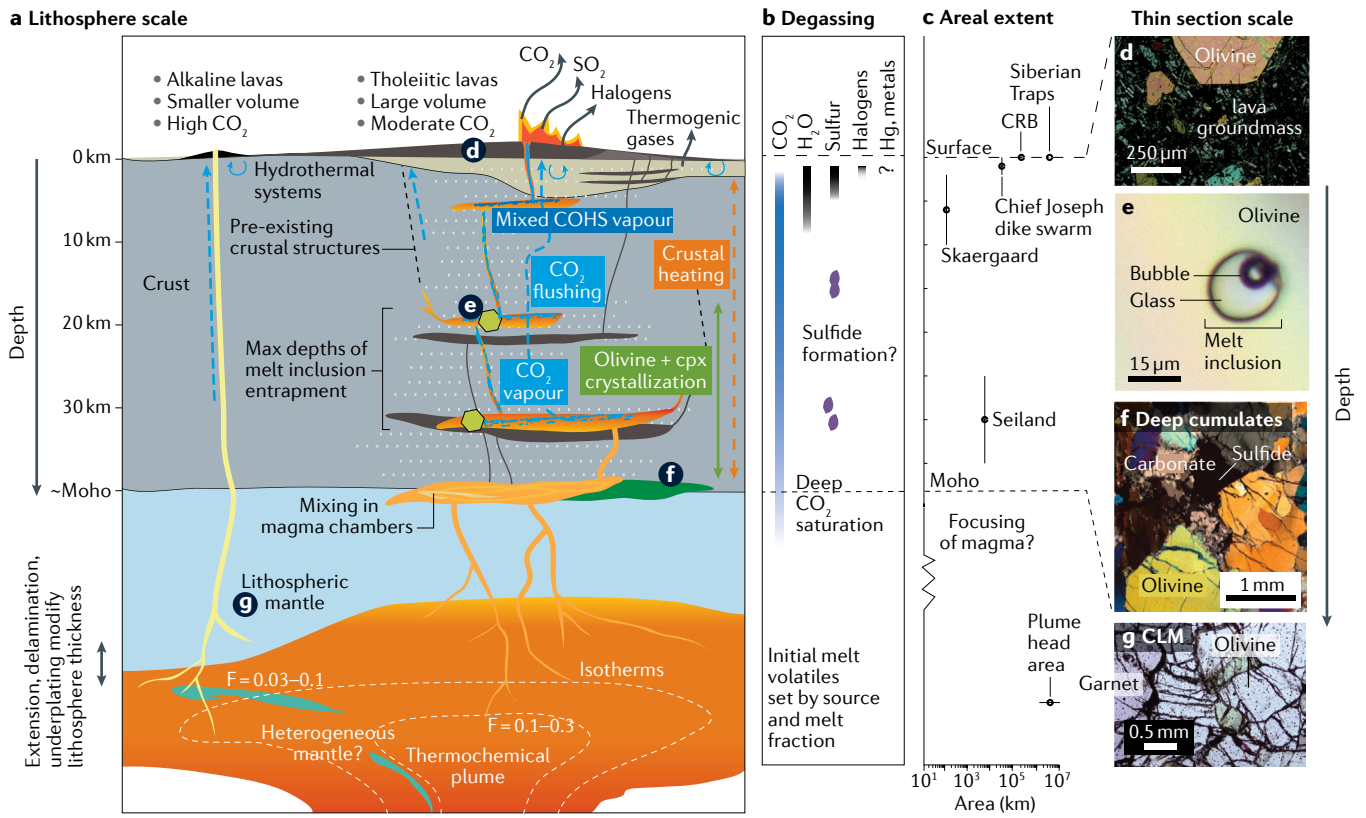

Fig. 1 | **Large igneous provinces represent Earth's largest magmatic events. a** | Cross section representing the crustal and upper mantle structure of a continental large igneous province approximately corresponding to the onset of main-phase volcanism, degassing depths (panel **b**) and areal extent for selected large igneous province lavas[241], dikes[90], magma reservoirs[80,242] and possible mantle plume head[18] (panel **c**). Representative thin section images correspond to labelled locations in panel **a**. **d** | Cross-polarized light photomicrograph of early Siberian Traps lava with olivine phenocrysts. **e** | Olivine-hosted melt inclusion with vapour bubble from the Deccan Traps. **f** | Carbonate-bearing cumulate from the Seiland igneous province. **g** | Garnet-bearing mantle xenolith from the Udachnaya kimberlite[214], which sampled the pre-Siberian Traps continental lithospheric mantle (CLM), revealing a halogen-rich reservoir[211] (BOX 1) with uncertain but potentially substantial carbon contents[10,11]. CRB, Columbia River Basalts. cpx, clinopyroxene. Panel **e** image courtesy of Andres Hernandez Nava. Panel **f** adapted with permission from REF.[81], Elsevier. Panel **g** image courtesy of Geoffrey Howarth.

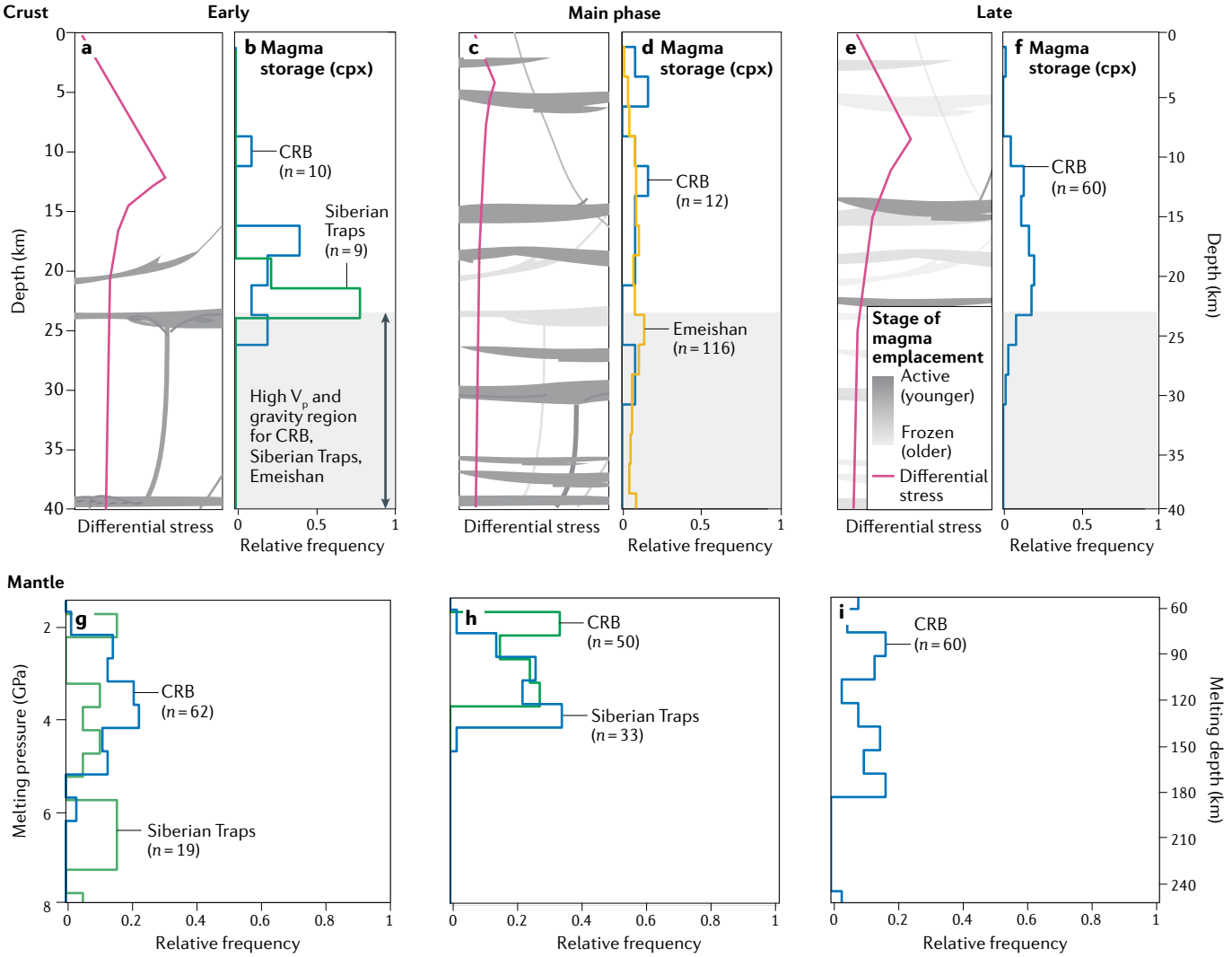

Fig. 2 | **Evolution of continental large igneous provinces.** Changing melting, storage and stress conditions from the mantle to the surface and through early, main-phase and late stages of large igneous province magmatism show how an extensive transcrustal plumbing system develops and wanes. **a**,**c**,**e** | Illustrations of changing storage depths (fading greyscale corresponds to magmas emplaced during prior stages) and qualitative lithospheric differential stress (pink curve) versus depth[243] modified to account for the hypothesized reduction in crustal strength from heating by large igneous province magmas. **b**,**d**,**f** | Magma storage pressures from geophysical constraints and clinopyroxene (cpx) barometry[244–247] (see REF.[248] for a review and equations used to calculate pressures from Siberian Traps cpx-melt compositions)[249]. Seismic and gravity data from the Siberian Traps, Columbia River Basalts (CRB) and Emeishan have been interpreted as evidence for dense intrusive bodies at 25–40-km depth[76,78,250,251] (shown as grey shaded boxes because the relative timing of intrusion is not constrained). **g–i** | Melting pressure estimates calculated with a major element thermobarometer[59], using compositional data from the Siberian Traps[55,63,180] and CRB[142,252]. For Siberian Traps, early panels include Ivakinsky, Syverminsky and Pravoboyarsky formations. For CRB, early panels include Steens and Imnaha formations, and late panels include Saddle Mountains Basalts.

Trace element
An element with concentration typically <1 wt%, such as rare-earth elements.

Partial melting
A fractional degree of melting, from 0% at the solidus to 100% at the liquidus.

Magma plumbing system
Transcrustal magma transport and storage networks that feed surface eruptions.

of thick lithosphere in oceanic settings. Thick lithosphere in some continental settings can stall basaltic melts at sufficient depths that they freeze as dense, delamination-prone eclogites. Indeed, there is evidence for a progression from shallow to deep melting in some oceanic LIPs. For example, trace element data from OJP and Kerguelen basalts hint at progressively decreasing degrees of melting[65–67], perhaps caused by magmatic thickening of the lithosphere or a waning plume.

Upper mantle to surface structure

LIP magmas are transported through, stored and stalled in the lithosphere, leading to deformation and hydrothermal activity in the crust.

Magmatic plumbing system. The mechanisms of melt transfer from asthenospheric melting zones to the base of the lithosphere are among the most poorly constrained aspects of the LIP magma plumbing system. At mid-ocean ridge settings[68], two-phase reactive compacting flow models suggest that initial grain-boundary melts can coalesce to form reactive melt channels that efficiently transport melt upwards from melting regions. Similar deep transport phenomena likely occur in mantle plume settings[69]. For both LIPs and oceanic ridges, variations in the depth of the lithosphere–asthenosphere boundary can act as an inverted catchment, focusing buoyant melts to thinner areas of the lithosphere[70,71].

Alternatively, active modification of the lower crust (including possible delamination in the case of the CRB)[72] and lithospheric mantle by ascending melts have been indicated by seismic constraints from receiver functions and surface wave radial anisotropy in the Deccan and CRB provinces[73,74]. Large-volume magma reservoirs are preserved as reflective, high-seismic-velocity layers with Moho-depth cumulative thicknesses of several to >10 km beneath the Deccan Traps, Siberian Traps, Emeishan Traps, OJP, Kerguelen, CRB, and High Arctic LIP[75–79] (FIG. 2). The extent to which these magma reservoirs were integrated versus a more complex network of stacked sills cannot be clearly resolved from available seismic data.

Rare, exhumed deep intrusions provide additional information on the structure of LIP plumbing systems. The ~580–560-Ma Seiland Igneous Province (northern Norway)[80] represents a possible exposure of a deep LIP magma plumbing system in fossil form. It comprises >17,000 km^3 of mafic, ultramafic, alkaline and felsic magmas that were emplaced at lower crustal pressures within gneissic metasedimentary and metaigneous country rocks[81]. The Seiland province has been interpreted as the roots of the Ediacaran-age Central Iapetus Magmatic Province[81]. The high proportion (1–5%) of carbonate and sulfide assemblages in the Seiland province point to the existence and mobility of exsolved volatiles in lower crustal magma transfer stations[80], supporting the view that volatiles could play a key role in modulating magma buoyancy, overpressure and further ascent into the crust[82–84].

These combined constraints are sufficient for postulating a conceptual framework for the spatial structure of LIP magma ascent (FIG. 1). Deep accumulation of channelized partial melt in the mantle results in fluid overpressure[83], associated with either compositional buoyancy (including deep CO_2 exsolution) or mass accumulation[83,85] that leads to fracturing and upward dike propagation. Growth of large magma reservoirs at a neutral buoyancy region near the base of the crust[48,77] (and potentially at shallower levels) is limited by structural destabilization and further dike propagation, driving continued ascent upward through the crust. Episodic reuse of transport pathways becomes more common in cool shallow crust, resulting in large composite dike and sill structures[13].

Intrusive to extrusive ratios. The magmatic intrusive to extrusive ratio represents a major uncertainty for relating surface volcanism to magma supply, not just for LIPs but across different magmatic settings[86–89]. The intrusive to extrusive ratio for LIPs has been estimated between 10:1 and 1:1 based on seismic, petrologic and gravity data, implying that most magmas do not erupt[75,77,90].

Seismic constraints on intrusive magmas at crustal depths omit frozen magmas in the mantle lithosphere, especially magmas that produce dense eclogites that can sink into the mantle[22,36,72]. Geodynamic simulations of the Deccan Traps and the NAIP[91,92] predict melt production of $4–10 \times 10^7$ km^3 during LIP emplacement. Comparison of these volumes of melt production from geodynamic modelling with Deccan and NAIP extrusive volume estimates[93,94] suggests as little as 1–5% by volume of mantle melts reached the surface during the main phase of magmatism. Interestingly, these same geodynamic modelling predictions of $10^7–10^8$ km^3 mantle melt align well with total volume estimates for large oceanic LIPs such as Ontong Java (~5×10^7 km^3 from REF.[95]), consistent with less delamination in oceanic settings.

Possible controls on magma storage depths and the balance between intrusion and eruption involve substantial interplay between magma supply rate, buoyancy (strongly influenced by volatiles) and time-evolving, temperature-dependent crustal rheology[96–99]. During early LIP emplacement, the middle to upper continental crust is expected to be cold and strong, favouring growth of magma chambers in the lower crust and mantle lithosphere (FIG. 2). Conduction of heat from the hot plume head, advection of heat by ascending magmas and latent heat associated with freezing of intrusions progressively alter the overall thermomechanical regime by modifying viscosity of the crust, stress state and mechanical anisotropy[100,101]. This interplay — which might also unfold similarly in rifts and arcs — likely contributes to a broadening distribution of storage depths during the main phase of magmatism relative to other phases of the LIP life cycle (FIG. 2b).

High magma supply to the lithosphere coincides with high degrees of melting. As these large volumes of hot basaltic magma transfer heat from the mantle[102], a broad swath of the crust heats sufficiently to easily accommodate growing magma reservoirs[103], further favouring staging in extensive crustal magma storage and transfer systems. Clinopyroxene barometry generally supports storage regions spanning the crust during the main phase of magmatism (FIG. 2). However, clinopyroxene barometry skews towards shallower storage depths than indicated by high-seismic-velocity regions (FIG. 2).

As magmas ascend into the brittle upper crust, dikes and sills become the dominant form of magma transport. Magnetic and mineral textures suggest that lateral rather than vertical magma flow becomes increasingly important at shallow depths[104]. Giant dike swarms facilitate lateral transfer of LIP magmas across distances of hundreds to thousands of kilometres[14,105]. Such lateral magma flow implies approximately neutral buoyancy[106]. In turn, magma buoyancy relative to wall-rocks as indicated by ascent or stalling can place bounds on volatile contents[82]. Interconnected sills and sill-fed dikes, such as those in the Ferrar Province[107], or dikes such as those in the CRB[90], can eventually breach the crust to feed surface flows[108–110].

Rapid ascent of alkaline magmas from the mantle. Alkaline magmas represent a small proportion of the overall volume of most LIPs because their lower degrees of melting yield smaller volumes of melt, and the geologic record of alkaline magmatism might be partially obscured by emplacement of more voluminous tholeiitic magmas. Nevertheless, alkaline rocks represent important markers for the extent and diversity of LIP melting conditions, including near-solidus melting on the margins of plumes and potential disruption of the CLM[11].

Intrusive to extrusive ratio
The proportion of primary magma that freezes upon ascent versus the volume that erupts on the surface.

Some alkaline magmas appear to largely bypass the tholeiitic crustal transport network, likely due to rapid ascent fuelled by high volatile contents[111]. Lower crustal or mantle xenoliths[112] found in some alkaline dikes and lavas attest to fast and relatively direct ascent from the depths at which these xenoliths were entrained. Such direct routes from the mantle could mean that alkaline rocks preserve clearer records of mantle processes than tholeiitic magmas that have experienced extensive but varying mixing, fractionation, and contamination in the crust, further motivating future investigation of the petrology and geochronology of alkaline LIP rocks.

Crustal deformation and surface topography. Interactions between mantle magma supply and the crust are recorded by time-evolving surface topography and crustal deformation. For example, classical plume models predict 1,000-km-scale doming associated with mantle plume impingement on the lithosphere[21]. Subsequent lateral spreading and rifting associated with thermal evolution of the crust during and post flood basalt emplacement can determine topographic uplift and erosion patterns[113]. Some Phanerozoic LIPs appear to display this progression (for example, Paraná–Etendeka)[114]. However, a consistent global LIP topographic signature is not clear. Indeed, 3D thermochemical plumes rising in a realistic mantle flow field can have complex topographic consequences[115–117]. Although not well studied, pre-plume topography may also give insight into the interplay of volcanism and landscape evolution. For example, surface waters and aquifers influence phreatomagmatic explosive activity[118–121] and pre-existing river networks may influence the distribution of flood lavas[122].

Perhaps the clearest evidence for magmatically driven dynamic topography comes from hotspots such as Galápagos, Iceland and Yellowstone[123], where uplift and subsidence exceeding the plume area has been attributed to flexure and lower crustal flow associated with magmatic loading[124,125]. Although obscured by lavas in many LIPs, numerous regional subsidence and faulting structures in the CRB have onset times coincident with main-phase magmatism[126]. Similar syn-eruptive subsidence features have been proposed in the Emeishan Traps[127].

The lateral deformation associated with LIP emplacement is even more profound. Although we do not focus on rifting here, flood basalt-scale volcanism has been hypothesized to play a role in rifting events[128–130] and supercontinent break-up[126,128,131]. Conversely, pre-existing crustal structures and stress state clearly impact the progression of LIP magmatism, as observed in the Deccan and CRB provinces[132].

LIP hydrothermal systems. The crust surrounding LIP magmas — both continental and oceanic — hosts hydrothermal activity that might, in some instances, rival mid-ocean ridge hydrothermal systems in scale[133], but LIP hydrothermal systems have received comparatively little attention. Weathering of mafic LIP rocks has been proposed as an important but controversial factor in Earth's silicate weathering cycle[134,135]. At mid-ocean ridges, hydrothermally mediated carbon sequestration in newly formed oceanic crust likely counterbalances CO_2 outgassing[136]. Oceanic LIP lavas are often pervasively altered[122,137], but how quickly this alteration takes place after emplacement is uncertain[138]. Improved understanding of alteration in LIP hydrothermal systems — in continental and oceanic settings — could be vital to assessing the role of LIPs for seawater chemistry and the long-term drawdown of atmospheric CO_2 in Earth's past[138].

Signatures of hydrothermal activity provide a powerful tool for inferring temporal progression of LIPs. For example, heat loss from CRB dikes drove fluid flow[133], and the pulsed cooling, heating and remelting of the ~300-km^3 LIP-related Skaergaard intrusive complex and its host rocks are encoded in crystal to km-scale variability of oxygen isotopes[139,140].

The tempo and death of LIPs

The multiscale transport and eruption tempo of LIP magmas highlights characteristic phases of the LIP life cycle. LIP stratigraphies, often comprising hundreds of lava flows[141], are generally subdivided into compositionally or stratigraphically distinct formations. In the case of the CRB (FIG. 3), these have been further subdivided into members that comprise mappable units with similar geochemistry, each containing a variable number of individual eruptions[142]. The variations in the tempo of LIP magmatism on these different scales are now discussed.

Tempo at the formation scale. Advances in the precision of U–Pb and Ar–Ar geochronology, improved consistency with magnetostratigraphy and refinements of erupted volumes provide increasing resolution of the pace of LIP magmatism[143–150]. Although there are differences between LIPs, high-precision geochronology suggests that many continental LIPs are characterized by a 'main phase' of tholeiitic eruptive activity spanning <1 Myr, during which most of the lava volume erupts. There is, however, notable complexity in cases such as the NAIP[151] and the Paraná–Etendeka[152], where evidence exists of marked precursory phases or protracted steady volcanism over longer (several Myr) timescales.

As geochronologic precision surpasses ±0.05%, variations in time-averaged volcanic output within the main phase have emerged, although hiatus durations are controversial[146,149,150,153]. Variations in the intensity of volcanic activity also find support from palaeomagnetic records[154–156] and coeval records of sedimentary Hg (REFS[5,157–159]), which leverage the role of volcanoes as a dominant source of environmental Hg to reconstruct province-scale activity intensity from sedimentary records.

Beyond the debate regarding the tempo of eruptive activity, a further key question is whether the main phase of volcanism is, or is not, the primary driver of the environmental crises associated with many LIPs (BOX 1). The pace of volatile release — rather than lava flux — is most directly and plausibly related to global environmental changes contemporaneous with LIP episodes. It remains unclear how these volatile fluxes evolve through the course of LIP magmatism.

Mantle xenoliths
Fragments of mantle rock entrained and transported in a magma — the presence of dense xenoliths in erupted volcanic rocks reflects sufficiently rapid ascent to keep them entrained.

Dynamic topography
Often defined as the time-dependent generation of surface relief from non-isostatic mantle or crustal flow.

Tempo
The tempo of magmatism is its pace, for example, how the intensity of magmatic activity varies through time — it often refers to the volume and frequency of eruptions at the surface.

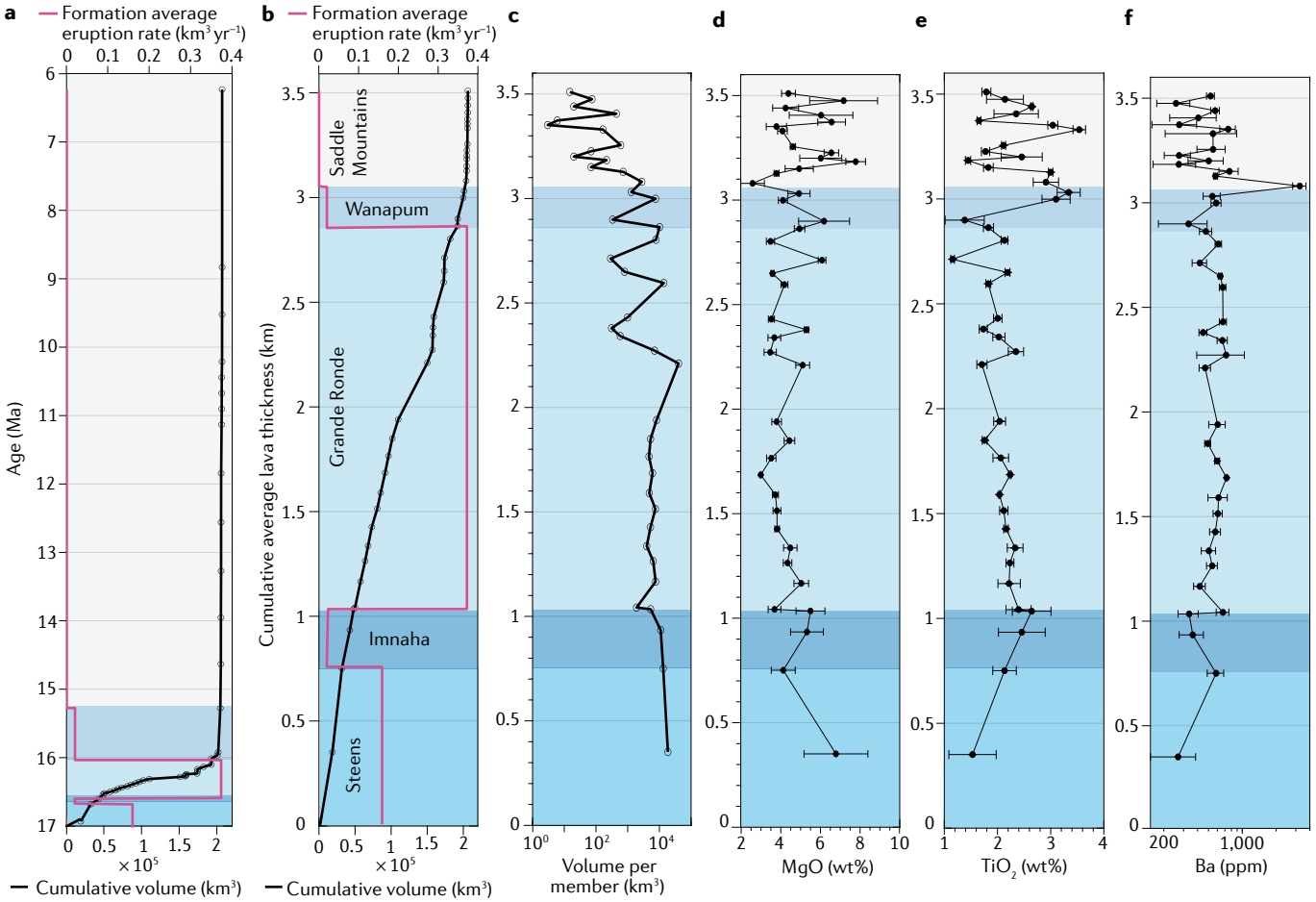

Fig. 3 | **Stratigraphy of the Columbia River Flood Basalts.** Detailed eruptive and chemical characterization make the Columbia River Basalts (CRB) a template for understanding the large igneous province life cycle. **a**,**b** | Cumulative erupted volume at the member level (black symbols and lines) and average eruption rate at the formation level (red curves) against time and average cumulative lava thickness, respectively. Note the short time interval of main-phase (Grande Ronde Formation) eruptions compared with that of the entire province. Classification and volumes come from REF.[142] and REF.[182] (for Steens), while dates come from REFS[145,146,253]. **c** | The average lava volume per member in log scale, suggesting substantial time evolution of crust–magma interactions that modulate eruption sizes, beginning during the main phase. **d**–**f** | Geochemical indices that track source variability and crustal interactions of CRB magmas. The relative constancy of early main-phase lavas account for nearly 50% of the total CRB eruptive output. Symbols and error bars represent the mean and range of geochemical values (the median number of samples per data point is 30). Geochemical data come from REFS[142,182,252].

Most continental LIPs also host more minor formations that predate and postdate the main phase. These formations, often alkaline in composition and less well preserved for older LIPs, record magmatism over a time period up to ~10 Myr or occasionally even longer[160]. LIP eruption fluxes seem to vary by more than an order of magnitude across formations[150]. It is an open question how such variations relate to transitions in the magnitude of excess mantle melting[161], to the effective crustal hydraulic connection between mantle source and the surface[83], or perhaps, in some cases, to external perturbations (such as the Chicxulub meteor impact in the case of Deccan Traps)[93].

In contrast with the more consistent <1-Myr duration of the main phase of continental LIPs, geochronology of oceanic LIPs reveals protracted high-flux magmatism spanning ~30 Myr in cases such as the Kerguelen Plateau[162] and Ontong Java[163]. Indeed, the Kerguelen Plateau has been linked to the 132-Ma Comei-Bunbury LIP[2,164], potentially extending the overall lifespan of the LIP to ~40 Myr. This divergence between the lifespan of continental and oceanic LIPs suggests that the lithosphere, and its influence on mantle melting, plays a strong role in modulating the tempo of surface volcanism.

Tempo at the member and individual eruption scale. Magmatic tempo on timescales of 10^3–10^4 years is likely mediated by magma chamber dynamics[83,84], which represent a nonlinear transfer function between slowly varying melt flux from the mantle and episodic surface eruptions. Melt aggregation also homogenizes magma compositions through cycles of recharge, eruption and fractional crystallization[48,165,166].

These transcrustal-scale magma dynamics control the environmental impacts of LIPs. For volcanic sulfate aerosols and halogens, which have lifetimes on the order of months to years in the stratosphere (much shorter than the full duration of main-phase magmatism), the duration and magnitude of emissions during individual eruptive events critically controls global climate

Box 1 | **LIPs and mass extinctions**

There is a well-established temporal correlation between the ages of Phanerozoic large igneous provinces (LIPs) and mass extinction and oceanic anoxic events. These links are substantiated by increasingly high-precision U–Pb and Ar–Ar geochronology of both LIP rocks and environmental perturbations determined from sedimentary records. Gases and particles released from magmas and country rocks during LIP volcanism have been proposed as key candidates for triggering these severe Earth system responses[6–8]. Impacts include: warming and ocean acidification from CO_2 release[272]; acid mist and short-term cooling from sulfur outgassing[167,168]; and ozone depletion from volcanic and metamorphic halogen compounds[217]. Changes in surface temperature have follow-on consequences for hydrology and ocean circulation[168]. On longer timescales (~1–10 Myr), weathering of LIP basalts can drawdown CO_2, perhaps drastically[135]. However, mechanistic insights into which of these processes are the most critical drivers of ecosystem collapse remains elusive. Earth system modelling employed to test the mechanisms responsible for observed environmental disruption depends on realistic volatile emission scenarios. While constraining such model inputs is challenging for LIPs, new datasets are becoming available that quantify volatile release from different parts of the LIP system (see the table below compiling data for the Siberian Traps). Other key parameters include eruption column height, extrusive versus intrusive flux and eruption versus hiatus durations.

Volatile	Estimated mass from magma[a]	Estimated mass from mantle	Estimated mass from CLM	Crust	Fluxes[b]	Possible consequences
CO_2	10^7–10^8 Mt[c]	1.7×10^8 Mt[d]	?	10^8 Mt[e]	10^2–10^4 Mt per year	Long-term warming, ocean acidification, changes to hydrology and ocean circulation
SO_2	12.6–15.6×10^6 Mt[f]	11.4–14.0×10^6 Mt[g]	?	10^6 Mt[g]	10^1–10^3 Mt per year	Transient cooling, acid mist, changes to hydrology and ocean circulation
Halogens	3.4–8.7×10^6 Mt HCl, 7.1–13.6×10^6 Mt HF[f]	1.8×10^7 Mt HCl[d]	8.7×10^6 Mt HCl, 2.3×10^4 Mt Br, 96 Mt I[h]	?	10^0–10^3 Mt per year HCl, HF 10^{-2}–10^0 Mt per year Br 10^{-4}–10^{-2} Mt per year I	Ozone depletion (from HCl, HBr, not F); local acidity
CH_4, organo-halogens, Hg, trace metals	?	?	?	?	?	Warming, ozone depletion, toxicity

1 Mt = 10^{12} g. CLM, continental lithospheric mantle. [a]Magma could include contributions from deep mantle, CLM and crust. [b]Fluxes are order-of-magnitude estimates based on magnitudes in preceding columns and assumed outgassing durations of 10^4–10^6 years. The 10^4-year duration is motivated by the cumulative duration of intense eruptive episodes assuming magma flux of 10^2 km^3 per year, consistent with palaeomagnetic evidence for emplacement of a large portion of the eruptive volume of the Siberian Traps across a cumulative duration of ~10^4 years[155]. [c]From modelling magma transport through carbon-rich upper crustal rocks[84]. [d]From thermomechanical modelling and petrological evidence for recycled oceanic crust[36]. [e]From crustal metamorphism[216]. [f]Based on melt inclusion measurements and 4×10^6 km^3 of extrusive rocks[249]. [g]From sulfur isotopes[264]. [h]From xenolith data scaled to HCl flux assuming the CLM flux dominates halogen emissions[211].

impacts[17,167,168]. Thus, constraining the tempo of LIP volcanism and degassing at the decadal to centennial scale is critical, but this temporal resolution remains beyond the limit of geochronology.

Evidence from lava flow morphology, palaeomagnetic measurements and chemical box modelling suggest emplacement rates of hundreds of km^3 per year (FIG. 4), lasting on the order of decades to centuries[154,155,169,170]. Additional constraints on the longevity of active eruption can be extracted from near-surface geothermometry of host rocks in the vicinity of feeder dikes, which record the time-evolving passage of magma. The Maxwell Lake feeder dike of the ~40,000-km^3 Wapshilla member of the CRB, representing multiple individual eruptions[142], has been constrained by petrography associated with partial melt of granitoid host rocks, resetting of palaeomagnetic directions, low-temperature (U–Th)/He thermochronology, oxygen isotopes and thermal modelling to have sustained magma flow for 1–6 years[171,172]. Given the known geometry and likely range of total erupted volume, this implies eruption rates of 1–8 km^3 per day for individual eruptions of the Wapshilla member associated with this dike[172,173].

Sedimentary layers interbedded with volcanic rocks provide a complementary view of eruptive tempo. Weathering boles intercalated with lavas in the Deccan Traps have been interpreted as a record of hiatuses in volcanic activity[174]. In the Central Atlantic Magmatic Province in eastern North America, well-developed sedimentary sequences several hundred metres thick are interbedded with unusually thick (reaching >100 m) lava flows[175,176]. By contrast, the main Siberian Traps volcanic sequences do not contain thick palaeosols or sedimentary layers[177]. The causes of these apparent differences in eruptive tempo amongst LIPs are not known.

Taken together, existing geochronology, thermochronology, palaeomagnetism, modelling and field evidence suggest that volcanic fluxes during the most intense episodes of volcanism can be orders of magnitude higher than the longer term average LIP volcanic fluxes constrained by geochronology (FIG. 4). This behaviour, on a smaller scale, is also observed in active settings such as Iceland and Hawaii, which supports the notion that processes modulating magma tempo during LIPs sit on a continuum of magmatic activity seen elsewhere.

Petrologic evolution encoded in eruptive stratigraphies. Exposures of kilometre-thick LIP volcanic sequences comprising hundreds of stacked lavas, along with drill cores, provide a unique record of geochemical evolution within and amongst LIPs. Geochemical progressions reflect the combined influences of mantle melt sources, fractionation, crustal contamination and post-emplacement alteration[178]. Variation in isotope, major and trace element compositions can be used to parse these processes[165]. Sr, Nd, Pb and Os isotope systems are

long-standing tools to trace mantle lithospheric and crustal contamination; Re–Os can also be used to resolve the timing of volcanism through seawater chemistry[55,151,179,180].

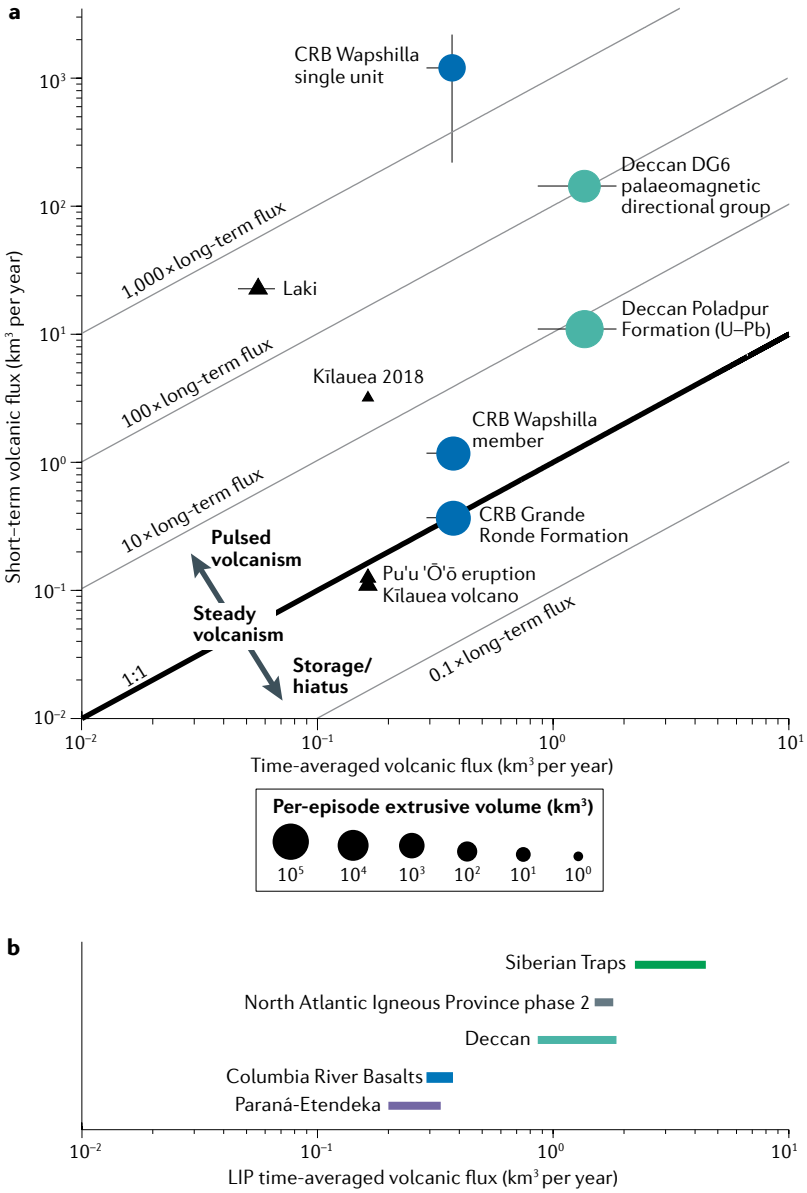

Fig. 4 | **The tempo of LIP magmatism varies across multiple timescales.** Shorter term volcanic fluxes can be orders of magnitude higher than mean volcanic fluxes during the main phase of large igneous province (LIP) volcanism. **a** | Shorter term volcanic fluxes are represented as the volume of individual units, members or formations, divided by their respective emplacement timescales[145,146,150,154,172,173,184]. Equivalent short-term and long-term fluxes imply steady volcanism (1:1 line). Episodes of short-term eruption rates much higher than long-term fluxes imply volcanic pulses. Intervals with lower volcanic fluxes than long-term rates imply storage or intrusion. At the scale of individual units or members, episodes of high flux likely reflect crustal magma transport. At the scale of formations, changes in mantle melting likely contribute to variations in volcanic flux. Deccan DG6 is a palaeomagnetic directional group[239]. Historic and modern episodes of volcanism are shown in panel **a** for comparison: Laki (15.1 km³ over 8 months[197] versus postglacial Iceland-wide average of 0.05 ± 0.01 km³ per year[254]) and Kīlauea (0.8 km³ over 3 months in 2018 (REF.[255]) and 4.4 km³ spanning the ~35-year Pu'u'Ō'ō eruption versus mean Kīlauea volcanic flux[256]). Circles represent LIP eruptions and triangles represent historical analogues. Error bars reflect the range in estimates of duration and volume. **b** | mean volcanic fluxes during the main phase of LIP volcanism are calculated as the volume divided by geochronologically determined duration[93,146,147,149,150,152,257].

Member-level geochemistry from the CRB (FIG. 3) shows a progression from primitive, high-MgO lavas to homogeneous, lower MgO Grande Ronde lavas, to the heterogeneous chemistry of late-phase Saddle Mountains Basalts. This late geochemical variability is also seen in the Deccan Traps in the form of alkaline eruptions millions of years after a much more homogeneous main phase[181] and, along with smaller eruption volumes, indicates that LIPs undergo a protracted waning phase.

Crystal chemical and textural records from LIPs hold vast unexploited potential. For example, many lavas contain crystal aggregates known as glomerocrysts[63,182], which, in other settings, have been interpreted as potential records of conditions in mushy reservoirs[183]. Other flood basalt lavas are strikingly phenocryst poor[184,185]. Interrogation of crystal-scale diffusion records[186,187] could dramatically improve constraints on ascent timescales and storage conditions of LIP magmas.

Eruptive style. The frequency of large silicic eruptions associated with dominantly basaltic LIPs remains an open question (see REFS[131,188] for reviews of dominantly silicic LIPs). However, silicic volcanism is a common observation. For example, the Paraná-Etendeka, CRB and Deccan provinces[189–191] all host subordinate silicic volcanism, as well the oceanic Kerguelen Plateau LIP, which culminated with episodes of explosive felsic volcanism[66]. Silicic eruptions have been linked to dispersal of Pb (REF.[192]) and produce copious ash that has been hypothesized to drive ocean fertilization[193].

Nonetheless, LIPs are generally dominated by basaltic styles of eruption. The degree of explosivity of basaltic LIP volcanism is an important question because sulfur and halogen injection altitude strongly control their lifetime in the atmosphere[167,194] and the eruption column and gas plume heights depend on eruptive style and intensity[195]. As the explosive products of LIP volcanism are only rarely preserved[196], interpretation of the style of LIP volcanism is often grounded in historical observations of basaltic fissure eruptions.

Based on detailed physical volcanology and first-hand accounts[197,198], the 1783–1784 Laki eruption in Iceland might be considered the 'type-example' LIP analogue: a sequence of 14 episodes over a 27-km en echelon set of dike segments, each episode characterized by a rapid waxing and longer waning of effusive flux, with violent fire-fountaining and Strombolian behaviour at the vent that produced minor tephra, along with prodigious amounts of lava totalling 14.7 ± 1 km³ over 8 months (FIG. 4). Vent-proximal explosive deposits, lava flow morphology (specifically, inflation features that promote long-distance transport)[199] and evidence for time-progressive localization of the feeder dike surface vent locations are all documented in LIPs[196,200]. Scaled experiments can capture complex fluid behaviour underlying vent evolution[201], and, in concert with multiphase modelling of bubbles and crystals in low-viscosity magmas[202,203], they offer a path to understanding the shallow magma dynamics that influence degassing and eruptive style.

Tephra deposits associated with the Roza unit of the CRB have been linked to fire fountains reaching

>1,000 m in height[196]. For comparison, Laki fire fountains reached an estimated 800–1,450 m (REF.[197]), and fire fountains from the Holuhraun 2014–2015 fissure eruption in Iceland reached approximately ~126 m (REF.[204]). Magma–water interactions can also produce explosive activity and voluminous proximal volcaniclastic rocks[205]. However, to date, few substantial airfall ash deposits have been linked with flood basalt activity, reflecting the weak preservation potential of such lithologies, the ash-poor character of fire-fountaining and relatively low eruption column heights.

Notable gas plumes can also loft above fissure-fed fire fountains. Laki fire fountains were estimated to have sustained eruption columns of up to 15-km altitude[177], based on historical reports from contemporary observers, facilitating sulfur injection to the upper troposphere and lower stratosphere. In oceanic plateaux, high water to magma ratios favour a combination of submarine lavas, hyaloclastites and intervals of subaerial volcanism accompanied by phreatomagmatic explosive activity[206].

Redistribution of volatiles

Volatile release during LIP activity represents one of the primary plausible links between magmatism and global environmental changes. Volatiles are also among the main drivers of eruptions. The sources, transfer and release of volatiles, and the petrologic controls that modulate fluxes to the atmosphere, are discussed here.

Volatile sources and budgets. LIP volatiles originate from the deep mantle, the CLM and the crust (through assimilation and metamorphism). Volatiles such as water, CO_2 and the halogens (with the exception of F)[207] are often strongly incompatible during mantle melting, corresponding to bulk distribution coefficients « 1. Therefore, the total mass of these volatiles extracted from a parcel of mantle undergoing melting does not change appreciably for melt fractions above a few percent. Instead, the larger volumes of melt produced during increasing degrees of melting simply dilute volatile concentrations in the resulting magma.

Consequently, it is the volume of mantle that undergoes melting and the initial volatile contents of the mantle source — rather than the volume of melt generated or the melt fraction — that primarily dictate the overall magnitude of volatile mobilization from the deep mantle. Mantle volatile concentrations could be heterogeneous during LIP melting. For example, estimated carbon concentrations in the deep and upper mantle are 50–500 ppm C and 10–30 ppm C, respectively[208], and mantle carbon and halogen enrichments due to recycled oceanic crust in the plume source have been suggested for the Siberian Traps[36].

In contrast with the incompatibility of CO_2, H_2O and Cl, the behaviour of S during mantle melting is more complex. Evidence from mantle xenoliths and diamond inclusions suggests that sulfides are common in the mantle; these sulfides likely control S concentrations in the melt until they are exhausted from the mantle source (~16% of aggregate fractional melting, assuming 140 ppm S in the mantle source)[209]. Main-phase tholeiitic magmas in which melt fractions can exceed 30% might no longer be in equilibrium with mantle sulfide; fluctuations in sulfur saturation state shallower in the magmatic plumbing system can further complicate the magmatic sulfur budget[209].

Ancient CLM is emerging as a major — but poorly quantified — reservoir of volatiles, including halogens, sulfur and both reduced and oxidized carbon, which accumulate on very long timescales due to percolation and freezing of melts and fluids from the underlying mantle[10,52,210–212]. LIP magmatism and rifting — sometimes operating in tandem — appear to be among the few geologic processes capable of disrupting and rejuvenating the long-lived CLM reservoir[213]. CLM contributions to LIP magma volatile contents could be substantial but are poorly constrained. Xenolith studies focusing on samples from kimberlites that predate and postdate LIP emplacement[211,214], as well as kimberlites directly associated with LIPs[215], offer promising means to gain snapshots of both the volatile budget of the CLM and the extent to which LIP activity can mobilize these volatiles. Percolation of low-degree melts on the margins of mantle plumes can also be a mechanism for replenishing CLM volatiles[10]. As oceanic plates lack >180-Ma lithospheric mantle, the lack of volatile release from the CLM may contribute to more muted climate consequences of oceanic plateaux relative to continental LIPs[210].

The crustal rocks into which LIP magmas intrude provide another potential explanation for differences in volatile release between LIPs. The degree of environmental stress caused by continental LIP volcanism has been correlated with the types of country rock intruded[216]. Crustal rocks such as carbonates, shales, hydrocarbon-bearing source rocks, evaporites and coals can release volatiles (for example, CO_2, hydrocarbons, halocarbons and Hg) to the environment via melting and assimilation into the magma or thermal metamorphism and direct release (BOX 1). By some estimates, carbon release owing to metamorphism can be an order of magnitude larger than that from mantle melting[216,217], though both mantle and crustal carbon release are poorly constrained and quantifying these fluxes for carbon, as well as for other volatiles, is a major focus of current research[11,94,218,219]. Other factors could also be important. For example, in addition to the absence of ancient CLM and fewer volatile-rich host rocks during emplacement of oceanic LIPs, degassing and atmospheric injection of sulfur, halogens and other volatiles are likely impeded during submarine eruptions.

Magnitude of volatile release. Determining the comparative release of volatiles from the deep mantle, the CLM and the crust — although critical to assessing why and how LIPs trigger surface environmental changes — is challenging (see BOX 1 for data from the Siberian Traps highlighting existing constraints from each of these sources and remaining gaps). Furthermore, due to changes in melting conditions and transport through the crust, volatile release is probably not evenly distributed through the span of LIP emplacement. Rather, release of CO_2, halogens and sulfur might each evolve semi-independently through the course of LIP magmatism.

Incompatible
Elements that are strongly enriched in the melt relative to solid phases during mantle melting, often due to ionic charge or radius that hinders their easy substitution into the structure of the solid phases that are present.

Bulk distribution coefficients
D_i, commonly abbreviated as $D_i = C_i^{solid}/C_i^{liq}$, for the concentration of a species i in a solid residue (C_i^{solid}) relative to in the liquid (C_i^{liq}). By definition, D_i « 1 for incompatible species.

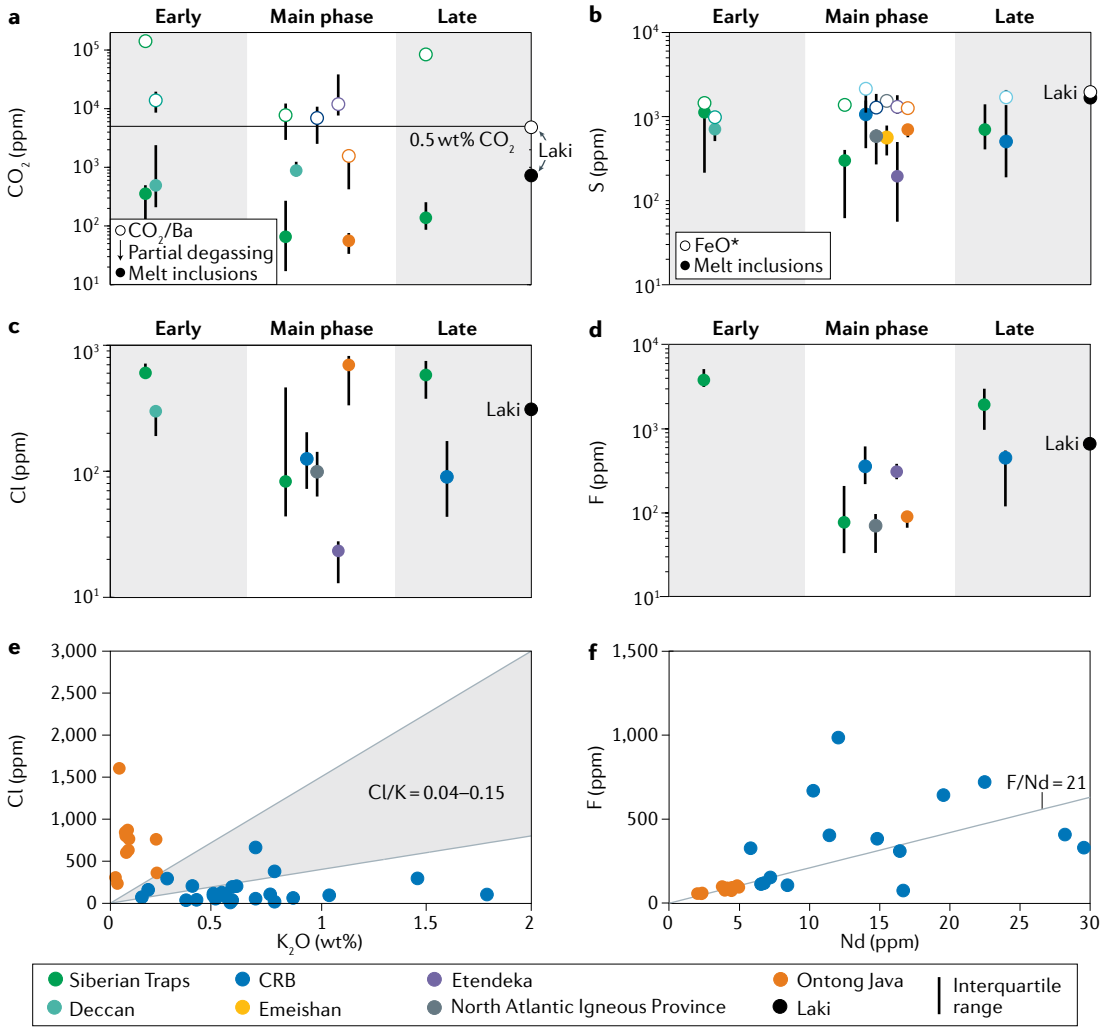

Fig. 5 | **Melt inclusion and proxy data track CO_2, S and halogen budgets in large igneous province magmas.** Evolving volatile fluxes during the large igneous province (LIP) life cycle link magma emplacement with environmental shifts (BOX 1). North Atlantic Igneous Province, Ontong Java and Emeishan data are plotted by default as main phase because the relative stratigraphies and/or distinctions between early, main-phase and late stages are unclear. **a** | CO_2 versus LIP phase. An assumed mantle CO_2/Ba ratio of ~140 from REFS[222,258] was used to estimate initial, pre-degassing magmatic CO_2 contents. Only samples with MgO > 7 wt% were used for this calculation, on the assumption that these would have experienced the least fractionation and/or assimilation that could modify Ba. A prior estimate of 0.5 wt% CO_2 (REF.[259]) derives from Icelandic and Hawaiian basalts. **b** | S versus LIP phase. Contents are shown from melt inclusions and estimated from melt inclusion FeO_{Total} (REF.[226]). For estimates using sulfur partitioning in clinopyroxene, see REF.[260]. **c**,**d** | Halogens versus LIP phase. **e**,**f** | Halogens versus K or Nd contents for Columbia River Basalts (CRB) and Ontong Java Plateau (OJP). K and Nd have been suggested as proxies for Cl and F, respectively, owing to similar behaviour during partial melting and crystallization, but have not been applied to LIP volatile calculations to date (see summary in REF.[207]). However, data from CRB[224] and OJP[67] suggest that there are large uncertainties in these proxies (for comparison, Cl/K of ~0.04–0.15 and F/Nd = 21 as suggested for ocean island basalts[223,261] are shown). Error bars represent the interquartile range. Data compilation is provided in Supplementary data Information, including data from the Siberian Traps[60,225,249,262–264], Deccan Traps[219,265,266], OJP[67], CRB[224,226,267], Emeishan[268], Etendeka[40,269] and North Atlantic Igneous Province[270] and Laki[220,271] (added to the right of the plots; Laki sulfur and halogen data are mean values).

Rehomogenization
The experimental reheating of crystals hosting recrystallized or bubble-bearing melt inclusions until inclusions melt, and then quenching to form homogeneous glass suitable for obtaining representative compositions by microanalysis.

Melt inclusions — tiny 'time capsules' of melt trapped inside crystals that can record pre-eruptive volatiles — provide snapshots of volatiles in LIP magmas (FIG. 5), subject to corrections for post-entrapment processes such as diffusion, shrinkage bubble formation and crystallization. Within melt inclusions, CO_2 often partitions into vapour bubbles (FIG. 1e) that likely commonly contain the majority of CO_2 (REFS[219–221]). Along with rehomogenization, Raman spectroscopy is emerging as an important technique to account for CO_2 in such bubbles to more accurately reconstruct CO_2 in ascending LIP magmas[218,219]. Even when corrected for post-entrapment processes, melt inclusions often trap already partially degassed melts — in particular, with respect to CO_2, which can saturate deep in the magmatic system (FIGS 2,5). Therefore, non-volatile trace elements that behave similarly to volatiles during melting can provide proxies for the initial, pre-degassing

melt concentrations (for example, Ba for CO_2 and Nd for F)[11,219,220,222,223]. Halogen data (FIG. 5c–f) suggest that oceanic LIPs could serve as a useful testing ground for this approach. Fluorine and Nd data from OJP[67] plot close to F/Nd = 21 (REF.[223]), whereas CRB F/Nd ratios[224] are more scattered, suggesting that oceanic plateaux can record mantle melting more cleanly.

Melt inclusions and other proxies can give insights into the variability of degassing between the different phases of LIPs. The Siberian Traps show evidence for relatively high CO_2 and halogens in melt inclusions from early and late alkaline magmas (FIG. 5), thought to originate from deep, low-degree melting[60,63,180,225] (FIG. 2). The extent to which other LIPs host similarly volatile-rich magmas is uncertain, largely due to generally sparse melt inclusion data for alkaline magmas. In general, CO_2 and halogens show substantial variability from LIP to LIP (FIG. 5). Sulfur concentrations are fairly consistent across LIPs, between phases and with proxy constraints (for example, FeO_{Total})[226], despite changes in melting conditions, suggesting buffering of sulfur concentrations during magma ascent[209].

Modes of volatile transfer and decoupling of volatiles from magma. Volatiles can be dissolved in, and thus move with, magma. However, there are multiple modes of volatile transport that effectively decouple volatile fluxes from eruption rates. CO_2 is expected to dominate the exsolved phase with increasing depth, owing to the strong pressure-dependence of CO_2 solubility in silicate melts (FIG. 1). Decoupled ascent of this CO_2-rich exsolved phase, known as CO_2 flushing, adds to the volatile mass of shallower magmas[227]. Even stronger decoupling between volcanism and outgassing is possible in the case of fluids or vapours — either exsolved from magmas or released via metamorphism of country rocks — that escape through high-permeability regions in the crust[96,216,228]. Very high non-eruptive CO_2 fluxes from modern basaltic systems[229,230] attest to the potential importance of this diffuse degassing.

Intrusive magmas and metamorphosed country rocks can also drive cryptic degassing, in which gas release exceeds that expected from erupted lava volumes[231]. Quantifying the relative importance of cryptic degassing — especially for intrusive LIP magmas, which could represent the majority of magma volume, and especially in relation to the overall evolution of the magmatic system — is a major unresolved challenge. Driven by changes in mantle-derived volatiles and ascent of exsolved fluids, the tempo of volatile release can decouple strongly from the tempo of volcanic eruptions at the surface[11]. This decoupling might explain apparent temporal offsets between peak volcanic fluxes and episodes of global warming during CRB and Deccan magmatism[145,219,231].

Sulfur exsolution into H_2O–CO_2-dominated bubbles can be complex. Magma redox, which is poorly constrained for LIPs, controls sulfur speciation and volatility[232], and influences saturation of a sulfide phase that buffers melt S concentrations[233]. Immiscible sulfide globules can scavenge metals and chalcophile elements[234,235]. Unlike dissolved volatiles, both bubbles and sulfide liquids can be mobile with respect to the melt, thereby, decoupling from volcanic output rates. While sulfides are dense and would re-sequester their volatiles upon sinking, attachment to bubbles has been proposed as a mechanism to buoy metal-bearing sulfides to reach the atmosphere under some circumstances[235]. In addition to sulfur flux, the climate response to sulfur outgassing also depends on emission duration, altitude, latitude and background climate[167,236].

CO_2 flushing
Refers to exsolution of CO_2-rich fluids at depth in the magmatic system, which then ascend and modify the balance of volatiles in shallower (typically more CO_2-depleted) magmas.

Diffuse degassing
Non-eruptive degassing via permeable pathways through the crust.

Cryptic degassing
Cryptic degassing is gas release due to intrusive or metamorphic degassing that causes total degassing to exceed expectations from magma volatile concentrations, and that can manifest as excess gas release during eruptions or as diffuse, non-eruptive degassing.

Magma redox
Refers to the balance between oxidation and reduction that determines the oxidation state of chemical species in the magma.

The evolution of LIP magmatic systems

LIP magmatic systems represent large-scale endmembers for volcanic activity on Earth and other planets. Variable magma supply and crustal rheology help define regimes of magma transport and storage[83] (FIG. 6) that offer generalizable insights into how volcanism works on large spatial and temporal scales. We suggest a conceptual model for the life cycle of continental LIPs to parallel thermomechanical changes hypothesized for other types of volcanic systems[237]. Initial mantle melts encounter a thermally immature crust, promoting rapid heating associated with freezing of smaller reservoirs. As the crust warms, ductile deformation increasingly dominates the crust's mechanical response to magma-induced stresses. Magma buoyancy, competing with time-evolving recharge from the mantle, results in hydraulic integration of storage zones, dike propagation and, ultimately, magma ascent[83,84], establishing a robust, transcrustal magma transport network during the main phase.

The onset, main phase and decline of the CRB is relatively well established. However, the extent to which other LIPs follow this progression remains unclear, in part, because high-precision geochronology tracking oceanic, alkaline and intrusive magmas is sparse. High-precision geochronologic data spanning the full duration of oceanic and continental LIPs — in particular, for alkaline, ultramafic and intrusive rocks — are needed to assess when LIPs follow, and when they depart from, the trajectory illustrated in FIG. 6. We expect the life cycle of oceanic LIPs to reflect a lower degree of thermal maturation of crustal host rocks due to efficient hydrothermal cooling of the thinner oceanic crust. Whether the progression of LIP eruptions can be linked to cyclic destabilization of individual[237], or perhaps many linked[238], magma chambers represents a key question required to further integrate LIPs into the spectrum of magmatism.

While intense debate has surrounded the origins of large-scale melting, less work has focused on the death of LIPs. Yet, both waning magma supply and more ductile crust — capable of accommodating new magma as intrusions — could reduce surface volcanism. This transition to a storage-dominated regime raises the possibility that emplacement and differentiation of Moho-depth intrusions could continue long after the cessation of most extrusive volcanic activity.

Summary and future perspectives

LIPs have a life cycle. Melting initiates, the first lavas erupt, large volumes of magma are emplaced rapidly (10^4–10^6 years for continental LIPs) in the lithosphere and at the surface with a tempo that varies from province to province. LIPs end over a longer waning phase (10^6–10^7 years for continental LIPs) with heterogeneous

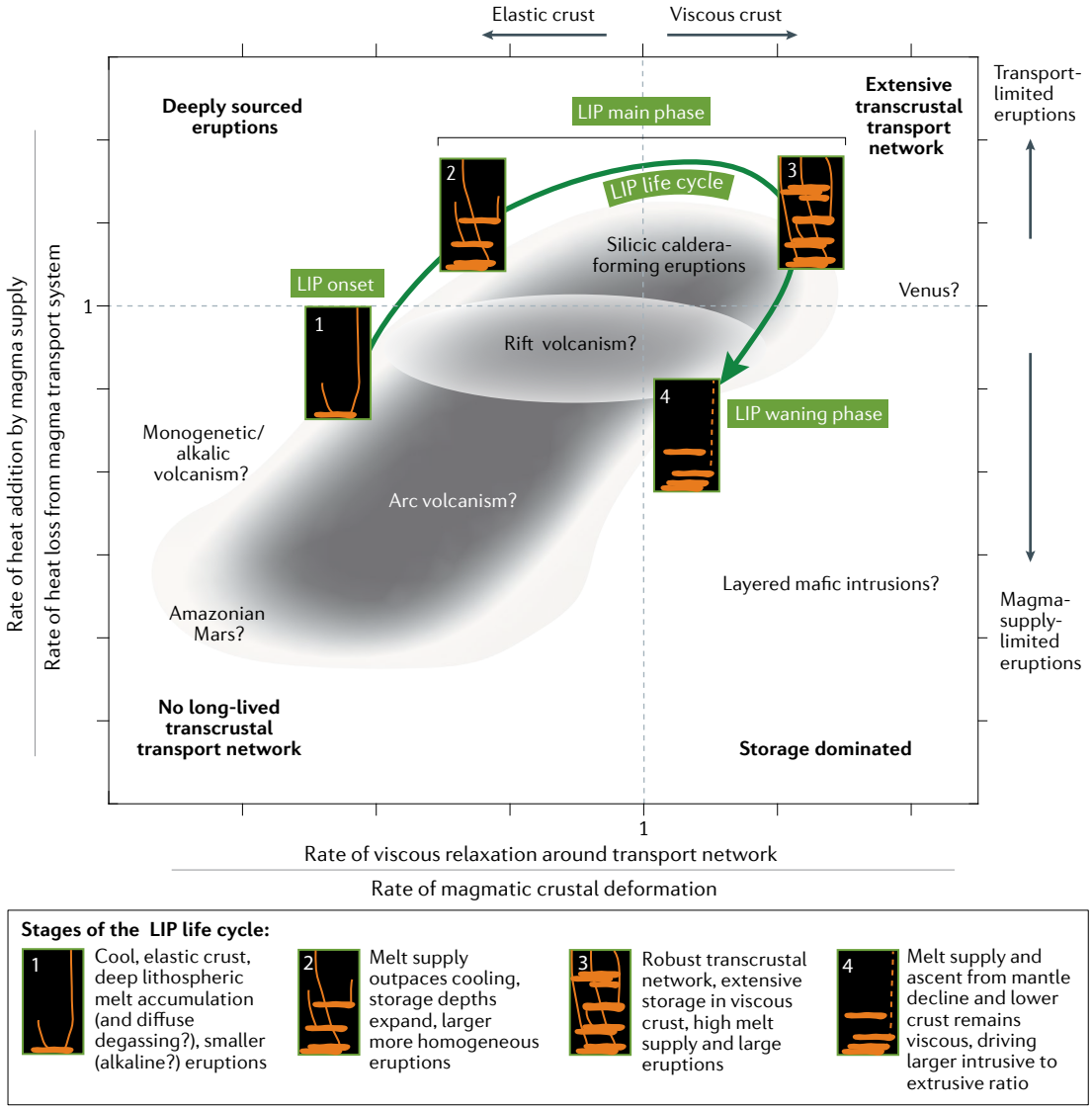

Fig. 6 | **Regime diagram tracking large igneous province evolution.** The life cycle of large igneous provinces (LIPs) and volcanism in other settings can be understood in terms of thermal and rheological controls of the crust on ascending mantle melts. LIP onset is characterized by high melt flux (compared with rift or arc settings on Earth) into a thermally immature crust, so resulting transport is governed by elastic and/or brittle behaviour of host rocks and heat loss to the crust. The LIP main phase is characterized by highest mantle melt fluxes. In continental settings, high magma supply interacts with a weakened crust, resulting in an enhanced ductile response of host rocks around intrusions, larger storage zones and a more robust transcrustal magma transport network. Rheological transition to a viscous crust could contribute to <1 Myr typical continental LIP main phase durations[83]. Large volume, prolonged shallow storage necessary to generate silicic caldera-forming eruptions[189] becomes rheologically feasible at this stage of continental LIPs. Waning phases of LIPs see declining mantle melt flux in a thermally evolved (but cooling) crust, possibly transitioning to a storage-dominated regime. Additional data from oceanic provinces are needed to understand whether and how their life cycle differs from continental LIPs. Figure adapted from REF.[103], Springer Nature Limited.

surface eruptions. Through this life cycle, LIPs mobilize volatiles from the deep mantle, mantle lithosphere and crust, underpinning proposed links with some of the most abrupt changes in surface environments in the past half-billion years of Earth's history.

The majority of continental LIP magmas likely do not erupt, but the nature and consequences of intrusive magmas are more poorly known than their erupted counterparts. Improved geophysical and petrologic constraints on intrusive LIP magmas are critically needed to understand their evolution, environmental repercussions and role in economic ore formation. In particular, there are opportunities to reconcile geodynamic modelling of melt generation and seismic imaging of the deeper crustal transport system with other constraints on the LIP life cycle.

Fluxes of LIP lava erupted at the surface are also highly variable and need further constraints, as estimates of maximum eruption rates during LIP activity span two orders of magnitude. The highest estimates imply volcanic fluxes of 10^2–10^3 km^3 per year[155,172,239], suggesting that the majority of lava volume from some LIPs

could have erupted over durations of $<10^4$ years. New techniques — for example, from palaeomagnetism or thermochronology — are needed to constrain durations and intensities of eruptive episodes and hiatuses.

LIP activity and continental rifting are among the few processes capable of dismembering and rejuvenating ancient continental lithospheric mantle. Therefore, they potentially play a unique role in solid Earth volatile cycling. Studies of alkaline magmas and mantle xenoliths — either directly associated with LIPs or erupted to the surface before or after LIP emplacement — offer complementary perspectives on the evolution of the mantle lithosphere and interactions with LIPs.

The redox state of the CLM is thought to be highly heterogeneous, and, therefore, data constraining the redox evolution of tholeiitic and alkaline LIP magmas could provide a unique window into mantle processes[52,212,240]. Volatiles such as CO_2, S, Cl and F are relatively easily measured through traditional analytical techniques, but existing datasets reveal broad diversity in volatile budgets of LIP magmas, motivating further efforts to constrain volatiles, particularly for oceanic plateaux and different stages of LIP activity. Developing new analytical techniques and datasets to track the behaviour and fluxes of lower concentration (but environmentally impactful) Hg, Br and trace metals are also needed to understand their degassing behaviour and imprint in sedimentary records[170,192,234].

Evolving volatile concentrations and the mobility of exsolved and metamorphic gases can cause the tempo of gas release to diverge from the extrusive flux. Tracking the transfer of volatiles within the magmatic system and through the crust, and exploring how the resulting volatile fluxes evolve through the life cycle of LIPs, provides a critical link between mantle melting and environmental perturbations. We urge adaptation of techniques from studies of volatiles in other volcanic settings (ranging from scaled experiments to multiphase modelling to trace element proxies for mantle volatiles) to investigate complex LIP systems.

Ultimately, we see a need to align increasingly high-resolution geochronologically and astrochronologically paced palaeoclimate records with similarly resolved timelines of magmatic processes to understand how LIPs can plausibly cause such profound changes in climate and why those shifts occur when they do. A central issue threading through these challenges is varying timescales: the processes that link melt generation in the mantle to surface outgassing have characteristic durations from seconds to millions of years. Understanding the multiple timescales that characterize LIP magmatic processes is an essential step towards reconciling large-scale volcanism with deep mantle drivers and disruption and change in Earth's surface climate.

Data availability

Data compilation used in FIG. 5 is available in a worksheet file (Supplementary data).

Published online: 23 November 2021

1. Bryan, S. E. & Ernst, R. E. Revised definition of large igneous provinces (LIPs). *Earth Sci. Rev.* **86**, 175–202 (2008).
2. Ernst, R. E. et al. in *Large Igneous Provinces: A Driver of Global Environmental and Biotic Changes* Ch. 1 (eds Ernst, R. E., Dickson, A. J. & Bekker, A.) 1–26 (Wiley, 2021).
3. Coffin, M. F. & Eldholm, O. Large igneous provinces: crustal structure, dimensions, and external consequences. *Rev. Geophys.* **32**, 1–36 (1994).
4. Ernst, R. E. *Large Igneous Provinces* (Cambridge Univ. Press, 2014).
5. Jones, M. T., Jerram, D. A., Svensen, H. H. & Grove, C. The effects of large igneous provinces on the global carbon and sulphur cycles. *Palaeogeogr. Palaeoclimatol. Palaeoecol.* **441**, 4–21 (2016).
6. Bond, D. P. & Wignall, P. B. Large igneous provinces and mass extinctions: an update. *Geol. Soc. Am. Spec. Pap.* **505**, 29–55 (2014).
7. Wignall, P. Large igneous provinces and mass extinctions. *Earth Sci. Rev.* **53**, 1–33 (2001).
8. Clapham, M. E. & Renne, P. R. Flood basalts and mass extinctions. *Annu. Rev. Earth Planet. Sci.* **47**, 275–303 (2019).
9. Courtillot, V. E. & Renne, P. R. On the ages of flood basalt events. *C.R. Geosci.* **335**, 113–140 (2003).
10. Foley, S. F. & Fischer, T. P. An essential role for continental rifts and lithosphere in the deep carbon cycle. *Nat. Geosci.* **10**, 897–902 (2017).
11. Black, B. A. & Gibson, S. A. Deep carbon and the life cycle of large igneous provinces. *Elements* **15**, 319–324 (2019).
12. Cashman, K. V., Sparks, R. S. & Blundy, J. D. Vertically extensive and unstable magmatic systems: a unified view of igneous processes. *Science* **355**, eaag3055 (2017).
13. Ernst, R. E., Liikane, D. A., Jowitt, S. M., Buchan, K. & Blanchard, J. A new plumbing system framework for mantle plume-related continental Large Igneous Provinces and their mafic-ultramafic intrusions. *J. Volcanol. Geotherm. Res.* **384**, 75–84 (2019).
14. Ernst, R., Grosfils, E. & Mege, D. Giant dike swarms: Earth, Venus, and Mars. *Annu. Rev. Earth Planet. Sci.* **29**, 489–534 (2001).
15. Buchan, K. L. & Ernst, R. E. Plumbing systems of large igneous provinces (LIPs) on Earth and Venus: investigating the role of giant circumferential and radiating dyke swarms, coronae and novae, and mid-crustal intrusive complexes. *Gondwana Res.* https://doi.org/10.1016/j.gr.2021.02.014 (2021).
16. Ernst, R. E. & Youbi, N. How Large Igneous Provinces affect global climate, sometimes cause mass extinctions, and represent natural markers in the geological record. *Palaeogeogr. Palaeoclimatol. Palaeoecol.* **478**, 30–52 (2017).
17. Self, S., Schmidt, A. & Mather, T. Emplacement characteristics, time scales, and volcanic gas release rates of continental flood basalt eruptions on Earth. *Geol. Soc. Am. Spec. Pap.* **505**, 319–337 (2014).
18. Campbell, I. H. Testing the plume theory. *Chem. Geol.* **241**, 153–176 (2007).
19. Foulger, G. R. in *Plates vs Plumes: A Geological Controversy* (Wiley-Blackwell, 2011).
20. Richards, M. A., Duncan, R. A. & Courtillot, V. E. Flood basalts and hot-spot tracks: plume heads and tails. *Science* **246**, 103–107 (1989).
21. Campbell, I. H. & Griffiths, R. W. Implications of mantle plume structure for the evolution of flood basalts. *Earth Planet. Sci. Lett.* **99**, 79–93 (1990).
22. Elkins-Tanton, L. T. & Hager, B. H. Melt intrusion as a trigger for lithospheric foundering and the eruption of the Siberian flood basalts. *Geophys. Res. Lett.* **27**, 3937–3940 (2000).
23. Jones, A. P., Price, G. D., Price, N. J., DeCarli, P. S. & Clegg, R. A. Impact induced melting and the development of large igneous provinces. *Earth Planet. Sci. Lett.* **202**, 551–561 (2002).
24. Coltice, N., Phillips, B., Bertrand, H., Ricard, Y. & Rey, P. Global warming of the mantle at the origin of flood basalts over supercontinents. *Geology* **35**, 391–394 (2007).
25. Gurnis, M. Large-scale mantle convection and the aggregation and dispersal of supercontinents. *Nature* **332**, 695–699 (1988).
26. French, S. W. & Romanowicz, B. Broad plumes rooted at the base of the Earth's mantle beneath major hotspots. *Nature* **525**, 95–99 (2015).
27. Tsekhmistrenko, M., Sigloch, K., Hosseini, K. & Barruol, G. A tree of Indo-African mantle plumes imaged by seismic tomography. *Nat. Geosci.* **14**, 612–619 (2021).
28. Stuart, F. M., Lass-Evans, S., Fitton, J. G. & Ellam, R. M. High $^3He/^4He$ ratios in picritic basalts from Baffin Island and the role of a mixed reservoir in mantle plumes. *Nature* **424**, 57–59 (2003).
29. Peters, B. J. et al. Helium–oxygen–osmium isotopic and elemental constraints on the mantle sources of the Deccan Traps. *Earth Planet. Sci. Lett.* **478**, 245–257 (2017).
30. Thompson, R. & Gibson, S. Transient high temperatures in mantle plume heads inferred from magnesian olivines in Phanerozoic picrites. *Nature* **407**, 502–506 (2000).
31. Herzberg, C. & Gazel, E. Petrological evidence for secular cooling in mantle plumes. *Nature* **458**, 619–622 (2009).
32. Coogan, L., Saunders, A. & Wilson, R. Aluminum-in-olivine thermometry of primitive basalts: evidence of an anomalously hot mantle source for large igneous provinces. *Chem. Geol.* **368**, 1–10 (2014).
33. Davies, D., Goes, S. & Sambridge, M. On the relationship between volcanic hotspot locations, the reconstructed eruption sites of large igneous provinces and deep mantle seismic structure. *Earth Planet. Sci. Lett.* **411**, 121–130 (2015).
34. Garnero, E. J., McNamara, A. K. & Shim, S. Continent-sized anomalous zones with low seismic velocity at the base of Earth's mantle. *Nat. Geosci.* **9**, 481–489 (2016).
35. Koppers, A. A. et al. Mantle plumes and their role in Earth processes. *Nat. Rev. Earth Environ.* **2**, 382–401 (2021).
36. Sobolev, S. V. et al. Linking mantle plumes, large igneous provinces and environmental catastrophes. *Nature* **477**, 312–316 (2011).
37. Mundl-Petermeier, A. et al. Anomalous ^{182}W in high $^3He/^4He$ ocean island basalts: fingerprints of Earth's core? *Geochim. Cosmochim. Acta* **271**, 194–211 (2020).
38. Trela, J. et al. The hottest lavas of the Phanerozoic and the survival of deep Archaean reservoirs. *Nat. Geosci.* **10**, 451–456 (2017).
39. Farnetani, C. G. & Richards, M. A. Numerical investigations of the mantle plume initiation model for

flood basalt events. *J. Geophys. Res. Solid Earth* **99**, 13813–13833 (1994).
40. Jennings, E. S., Gibson, S. A. & Maclennan, J. Hot primary melts and mantle source for the Paraná-Etendeka flood basalt province: new constraints from Al-in-olivine thermometry. *Chem. Geol.* **529**, 119287 (2019).
41. Spice, H. E., Fitton, J. G. & Kirstein, L. A. Temperature fluctuation of the Iceland mantle plume through time. *Geochem. Geophys. Geosyst.* **17**, 243–254 (2016).
42. Kamenetsky, V. S., Chung, S., Kamenetsky, M. B. & Kuzmin, D. V. Picrites from the Emeishan Large Igneous Province, SW China: a compositional continuum in primitive magmas and their respective mantle sources. *J. Petrol.* **53**, 2095–2113 (2012).
43. Lightfoot, P. C. et al. Remobilization of the continental lithosphere by a mantle plume - Major-element, trace-element, and Sr-isotope, Nd-isotope, and Pb-isotope evidence from picritic and tholeiitic lavas of the Noril'sk district, Siberian Trap, Russia. *Contrib. Mineral. Petrol.* **114**, 171–188 (1993).
44. Camp, V. E. & Hanan, B. B. A plume-triggered delamination origin for the Columbia River Basalt Group. *Geosphere* **4**, 480–495 (2008).
45. Pearce, J. A., Ernst, R. E., Peate, D. W. & Rogers, C. LIP printing: use of immobile element proxies to characterize Large Igneous Provinces in the geologic record. *Lithos* **392-393**, 106068 (2021).
46. Shorttle, O. & Maclennan, J. Compositional trends of Icelandic basalts: implications for short–length scale lithological heterogeneity in mantle plumes. *Geochem. Geophys. Geosyst.* **12**, 11008 (2011).
47. Kent, A. et al. Mantle heterogeneity during the formation of the North Atlantic Igneous Province: constraints from trace element and Sr–Nd–Os–O isotope systematics of Baffin Island picrites. *Geochem. Geophys. Geosyst.* **5**, Q11004 (2004).
48. Cox, K. A model for flood basalt vulcanism. *J. Petrol.* **21**, 629–650 (1980).
49. Alt, J. C. et al. Recycling of water, carbon, and sulfur during subduction of serpentinites: a stable isotope study of Cerro del Almirez, Spain. *Earth Planet. Sci. Lett.* **327**, 50–60 (2012).
50. Hofmann, A. W. & White, W. M. Mantle plumes from ancient oceanic crust. *Earth Planet. Sci. Lett.* **57**, 421–436 (1982).
51. Sobolev, A. V. et al. The amount of recycled crust in sources of mantle-derived melts. *Science* **316**, 412–417 (2007).
52. Stagno, V., Ojwang, D. O., McCammon, C. A. & Frost, D. J. The oxidation state of the mantle and the extraction of carbon from Earth's interior. *Nature* **493**, 84–88 (2013).
53. Cabral, R. A. et al. Anomalous sulphur isotopes in plume lavas reveal deep mantle storage of Archaean crust. *Nature* **496**, 490–493 (2013).
54. Wang, X. J. et al. Recycled ancient ghost carbonate in the Pitcairn mantle plume. *Proc. Natl Acad. Sci. USA* **115**, 8682–8687 (2018).
55. Wooden, J. L. et al. Isotopic and trace-element constraints on mantle and crustal contributions to Siberian continental flood basalts, Noril'sk area, Siberia. *Geochim. Cosmochim. Acta* **57**, 3677–3704 (1993).
56. Gibson, S., Thompson, R. & Day, J. Timescales and mechanisms of plume–lithosphere interactions: $^{40}Ar/^{39}Ar$ geochronology and geochemistry of alkaline igneous rocks from the Paraná–Etendeka large igneous province. *Earth Planet. Sci. Lett.* **251**, 1–17 (2006).
57. Herzberg, C. & O'hara, M. Plume-associated ultramafic magmas of Phanerozoic age. *J. Petrol.* **43**, 1857–1883 (2002).
58. White, R. & McKenzie, D. Mantle plumes and flood basalts. *J. Geophys. Res.Solid Earth* **100**, 17543–17585 (1995).
59. Lee, C. A., Luffi, P., Plank, T., Dalton, H. & Leeman, W. P. Constraints on the depths and temperatures of basaltic magma generation on Earth and other terrestrial planets using new thermobarometers for mafic magmas. *Earth Planet. Sci. Lett.* **279**, 20–33 (2009).
60. Sobolev, A. V., Sobolev, S. V., Kuzmin, D., Malitch, K. & Petrunin, A. Siberian meimechites: origin and relation to flood basalts and kimberlites. *Russ. Geol. Geophys.* **50**, 999–1033 (2009).
61. Herzberg, C. Partial melting below the Ontong Java Plateau. *Geol. Soc.* **229**, 179–183 (2004).
62. White, R. & McKenzie, D. Magmatism at rift zones: the generation of volcanic continental margins and flood basalts. *J. Geophys. Res. Solid Earth* **94**, 7685–7729 (1989).
63. Fedorenko, V., Czamanske, G., Zen'ko, T., Budahn, J. & Siems, D. Field and geochemical studies of the melilite-rearing Arydzhangsky Suite, and an overall perspective on the Siberian alkaline-ultramafic flood-volcanic rocks. *Int. Geol. Rev.* **42**, 769–804 (2000).
64. Simonetti, A. & Neal, C. R. In-situ chemical, U-Pb dating, and Hf isotope investigation of megacrystic zircons, Malaita (Solomon Islands): evidence for multi-stage alkaline magmatic activity beneath the Ontong Java Plateau. *Earth Planet. Sci. Lett.* **295**, 251–261 (2010).
65. Frey, F. A. et al. Temporal geochemical trends in Kerguelen Archipelago basalts: evidence for decreasing magma supply from the Kerguelen plume. *Chem. Geol.* **164**, 61–80 (2000).
66. Frey, F. A. et al. Origin and evolution of a submarine large igneous province: the Kerguelen Plateau and Broken Ridge, southern Indian Ocean. *Earth Planet. Sci. Lett.* **176**, 73–89 (2000).
67. Jackson, M. G. et al. Ultra-depleted melts in olivine-hosted melt inclusions from the Ontong Java Plateau. *Chem. Geol.* **414**, 124–137 (2015).
68. Weatherley, S. M. & Katz, R. F. Melting and channelized magmatic flow in chemically heterogeneous, upwelling mantle. *Geochem. Geophys. Geosyst.* **13**, Q0AC18 (2012).
69. Stracke, A. A process-oriented approach to mantle geochemistry. *Chem. Geol.* **579**, 120350 (2021).
70. Thompson, R. & Gibson, S. A. Subcontinental mantle plumes, hotspots and pre-existing thinspots. *J. Geol. Soc.* **148**, 973–977 (1991).
71. Sleep, N. H. Lateral flow and ponding of starting plume material. *J. Geophys. Res. Solid Earth* **102**, 10001–10012 (1997).
72. Gao, H. Crustal seismic structure beneath the source area of the Columbia River flood basalt: bifurcation of the Moho driven by lithosphere delamination. *Geophys. Res. Lett.* **42**, 9764–9771 (2015).
73. Sharma, J., Kumar, M. R., Roy, K. S., Pal, S. & Roy, P. Low-velocity zones and negative radial anisotropy beneath the plume perturbed northwestern Deccan volcanic province. *J. Geophys. Res. Solid Earth* **126**, e2020JB020295 (2021).
74. Niday, W. & Humphreys, E. Complex upper mantle anisotropy in the Pacific Northwest: evidence from SKS splitting. *Earth Planet. Sci. Lett.* **540**, 116264 (2020).
75. Ridley, V. A. & Richards, M. A. Deep crustal structure beneath large igneous provinces and the petrologic evolution of flood basalts. *Geochem. Geophys. Geosyst.* **11**, Q09006 (2010).
76. Catchings, R. & Mooney, W. Crustal structure of the Columbia Plateau: evidence for continental rifting. *J. Geophys. Res. Solid Earth* **93**, 459–474 (1988).
77. Thybo, H. & Artemieva, I. Moho and magmatic underplating in continental lithosphere. *Tectonophysics* **609**, 605–619 (2013).
78. Davenport, K., Hole, J., Tikoff, B., Russo, R. & Harder, S. A strong contrast in crustal architecture from accreted terranes to craton, constrained by controlled-source seismic data in Idaho and eastern Oregon. *Lithosphere* **9**, 325–340 (2017).
79. Oakey, G. & Saltus, R. Geophysical analysis of the Alpha–Mendeleev ridge complex: characterization of the High Arctic Large Igneous Province. *Tectonophysics* **691**, 65–84 (2016).
80. Larsen, R. B. et al. Portrait of a giant deep-seated magmatic conduit system: the Seiland Igneous Province. *Lithos* **296**, 600–622 (2018).
81. Grant, T. B. et al. Anatomy of a deep crustal volcanic conduit system; the Reinfjord ultramafic complex, Seiland Igneous Province, northern Norway. *Lithos* **252**, 200–215 (2016).
82. Lange, R. A. Constraints on the preeruptive volatile concentrations in the Columbia River flood basalts. *Geology* **30**, 179–182 (2002).
83. Karlstrom, L. & Richards, M. On the evolution of large ultramafic magma chambers and timescales for flood basalt eruptions. *J. Geophys. Res. Solid Earth* **116**, B08216 (2011).
84. Black, B. A. & Manga, M. Volatiles and the tempo of flood basalt magmatism. *Earth Planet. Sci. Lett.* **458**, 130–140 (2017).
85. Farnetani, C. G., Richards, M. A. & Ghiorso, M. S. Petrological models of magma evolution and deep crustal structure beneath hotspots and flood basalt provinces. *Earth Planet. Sci. Lett.* **143**, 81–94 (1996).
86. White, S. M., Crisp, J. A. & Spera, F. J. Long-term volumetric eruption rates and magma budgets. *Geochem. Geophys. Geosyst.* **7**, Q03010 (2006).
87. Crisp, J. A. Rates of magma emplacement and volcanic output. *J. Volcanol. Geotherm. Res.* **20**, 177–211 (1984).
88. Tierney, C. R., Schmitt, A. K., Lovera, O. M. & de Silva, S. L. Voluminous plutonism during volcanic quiescence revealed by thermochemical modeling of zircon. *Geology* **44**, 683–686 (2016).
89. Ward, K. M., Delph, J. R., Zandt, G., Beck, S. L. & Ducea, M. N. Magmatic evolution of a Cordilleran flare-up and its role in the creation of silicic crust. *Sci. Rep.* **7**, 9047 (2017).
90. Morriss, M. C., Karlstrom, L., Nasholds, M. W. & Wolff, J. A. The Chief Joseph dike swarm of the Columbia River flood basalts, and the legacy data set of William H. Taubeneck. *Geosphere* **16**, 1082–1106 (2020).
91. Glišović, P. & Forte, A. M. On the deep-mantle origin of the Deccan Traps. *Science* **355**, 613–616 (2017).
92. Glišović, P. & Forte, A. M. Two deep-mantle sources for Paleocene doming and volcanism in the North Atlantic. *Proc. Natl Acad. Sci. USA* **116**, 13227–13232 (2019).
93. Richards, M. A. et al. Triggering of the largest Deccan eruptions by the Chicxulub impact. *Geol. Soc. Am. Bull.* **127**, 1507–1520 (2015).
94. Saunders, A. D. Two LIPs and two Earth-system crises: the impact of the North Atlantic Igneous Province and the Siberian Traps on the Earth-surface carbon cycle. *Geol. Mag.* **153**, 201–222 (2016).
95. Gladczenko, T. P., Coffin, M. F. & Eldholm, O. Crustal structure of the Ontong Java Plateau: modeling of new gravity and existing seismic data. *J. Geophys. Res. Solid Earth* **102**, 22711–22729 (1997).
96. Mittal, T. & Richards, M. A. Volatile degassing from magma chambers as a control on volcanic eruptions. *J. Geophys. Res. Solid Earth* **124**, 7869–7901 (2019).
97. Jellinek, A. M. & DePaolo, D. J. A model for the origin of large silicic magma chambers: precursors of caldera-forming eruptions. *Bull. Volcanol.* **65**, 363–381 (2003).
98. Colón, D. P., Bindeman, I. N. & Gerya, T. V. Understanding the isotopic and chemical evolution of Yellowstone hot spot magmatism using magmatic-thermomechanical modeling. *J. Volcanol. Geotherm. Res.* **370**, 13–30 (2019).
99. Huber, C., Townsend, M., Degruyter, W. & Bachmann, O. Optimal depth of subvolcanic magma chamber growth controlled by volatiles and crust rheology. *Nat. Geosci.* **12**, 762–768 (2019).
100. Perry-Houts, J. & Karlstrom, L. Anisotropic viscosity and time-evolving lithospheric instabilities due to aligned igneous intrusions. *Geophys. J. Int.* **216**, 794–802 (2019).
101. Keller, T., May, D. A. & Kaus, B. J. Numerical modelling of magma dynamics coupled to tectonic deformation of lithosphere and crust. *Geophys. J. Int.* **195**, 1406–1442 (2013).
102. Petford, N. Rheology of granitic magmas during ascent and emplacement. *Annu. Rev. Earth Planet. Sci.* **31**, 399–427 (2003).
103. Karlstrom, L., Paterson, S. R. & Jellinek, A. M. A reverse energy cascade for crustal magma transport. *Nat. Geosci.* **10**, 604–608 (2017).
104. Magee, C., Ernst, R. E., Muirhead, J., Phillips, T. & Jackson, C. A. L. in *Dyke Swarms of the World: A Modern Perspective* (eds Srivastava, R., Ernst, R. & Peng, P.) 45–85 (Springer, 2019).
105. Wolff, J., Ramos, F., Hart, G., Patterson, J. & Brandon, A. Columbia River flood basalts from a centralized crustal magmatic system. *Nat. Geosci.* **1**, 177–180 (2008).
106. Parfitt, E. & Head, J. Buffered and unbuffered dike emplacement on Earth and Venus: implications for magma reservoir size, depth, and rate of magma replenishment. *Earth Moon Planets* **61**, 249–281 (1993).
107. Muirhead, J. D., Airoldi, G., Rowland, J. V. & White, J. D. Interconnected sills and inclined sheet intrusions control shallow magma transport in the Ferrar large igneous province, Antarctica. *Bulletin* **124**, 162–180 (2012).
108. Muirhead, J. D., Airoldi, G., White, J. D. & Rowland, J. V. Cracking the lid: sill-fed dikes are the likely feeders of flood basalt eruptions. *Earth Planet. Sci. Lett.* **406**, 187–197 (2014).
109. Block, K. A., Steiner, J. C., Puffer, J. H., Jones, K. M. & Goldstein, S. L. Evolution of late stage differentiates in the Palisades Sill, New York and New Jersey. *Lithos* **230**, 121–132 (2015).
110. Reidel, S. P. & Tolan, T. L. Eruption and emplacement of flood basalt: an example from the large-volume

Teepee Butte Member, Columbia River Basalt Group. *Geol. Soc. Am. Bull.* **104**, 1650–1671 (1992).
111. Arndt, N., Chauvel, C., Czamanske, G. & Fedorenko, V. Two mantle sources, two plumbing systems: tholeiitic and alkaline magmatism of the Maymecha River basin, Siberian flood volcanic province. *Contrib. Mineral. Petrol.* **133**, 297–313 (1998).
112. Dessai, A., Markwick, A., Vaselli, O. & Downes, H. Granulite and pyroxenite xenoliths from the Deccan Trap: insight into the nature and composition of the lower lithosphere beneath cratonic India. *Lithos* **78**, 263–290 (2004).
113. Friedrich, A. M. et al. Stratigraphic framework for the plume mode of mantle convection and the analysis of interregional unconformities on geological maps. *Gondwana Res.* **53**, 159–188 (2018).
114. Krob, F. C., Glasmacher, U. A., Bunge, H., Friedrich, A. M. & Hackspacher, P. C. Application of stratigraphic frameworks and thermochronological data on the Mesozoic SW Gondwana intraplate environment to retrieve the Paraná-Etendeka plume movement. *Gondwana Res.* **84**, 81–110 (2020).
115. Lin, S. & van Keken, P. E. Multiple volcanic episodes of flood basalts caused by thermochemical mantle plumes. *Nature* **436**, 250–252 (2005).
116. Burov, E. & Gerya, T. Asymmetric three-dimensional topography over mantle plumes. *Nature* **513**, 85–89 (2014).
117. Leng, W. & Zhong, S. Surface subsidence caused by mantle plumes and volcanic loading in large igneous provinces. *Earth Planet. Sci. Lett.* **291**, 207–214 (2010).
118. Black, B. A., Weiss, B. P., Elkins-Tanton, L. T., Veselovskiy, R. V. & Latyshev, A. Siberian Traps volcaniclastic rocks and the role of magma-water interactions. *Geol. Soc. Am. Bull.* **127**, 1437–1452 (2015).
119. Czamanske, G. K., Gurevitch, A., Fedorenko, V. & Simonov, O. Demise of the Siberian plume: paleogeographic and paleotectonic reconstruction from the prevolcanic and volcanic record, north-central Siberia. *Int. Geol. Rev.* **40**, 95–115 (1998).
120. Polozov, A., Svensen, H. & Planke, S. Formation of Phreatomagmatic Pipes in the Tunguska Basin (Siberia, Russia) during the end-Permian. *Geophys. Res. Abstr.* **12**, EGU2010-13128 (2010).
121. Peate, I. U. & Bryan, S. E. Re-evaluating plume-induced uplift in the Emeishan large igneous province. *Nat. Geosci.* **1**, 625–629 (2008).
122. Neal, C. R., Mahoney, J. J. & Chazey III, W. J. Mantle sources and the highly variable role of continental lithosphere in basalt petrogenesis of the Kerguelen Plateau and Broken Ridge LIP: results from ODP Leg 183. *J. Petrol.* **43**, 1177–1205 (2002).
123. McQuarrie, N. & Rodgers, D. W. Subsidence of a volcanic basin by flexure and lower crustal flow: the eastern Snake River Plain, Idaho. *Tectonics* **17**, 203–220 (1998).
124. Jones, S. & Maclennan, J. Crustal flow beneath Iceland. *J. Geophys. Res. Solid Earth* **110**, B09410 (2005).
125. Orellana-Rovirosa, F. & Richards, M. Evidence and models for lower crustal flow beneath the Galápagos platform. *Geochem. Geophys. Geosyst.* **17**, 113–142 (2016).
126. Mitchell, R. N. et al. The supercontinent cycle. *Nat. Rev. Earth Environ.* **2**, 358–374 (2021).
127. Zhu, J. et al. Weak vertical surface movement caused by the ascent of the Emeishan mantle anomaly. *J. Geophys. Res. Solid Earth* **123**, 1018–1034 (2018).
128. Courtillot, V., Jaupart, C., Manighetti, I., Tapponnier, P. & Besse, J. On causal links between flood basalts and continental breakup. *Earth Planet. Sci. Lett.* **166**, 177–195 (1999).
129. Planke, S., Symonds, P. A., Alvestad, E. & Skogseid, J. Seismic volcanostratigraphy of large-volume basaltic extrusive complexes on rifted margins. *J. Geophys. Res. Solid Earth* **105**, 19335–19351 (2000).
130. Hooper, P. R. The timing of crustal extension and the eruption of continental flood basalts. *Nature* **345**, 246–249 (1990).
131. Bryan, S. E. & Ferrari, L. Large igneous provinces and silicic large igneous provinces: progress in our understanding over the last 25 years. *GSA Bull.* **125**, 1053–1078 (2013).
132. Vanderkluysen, L., Mahoney, J. J., Hooper, P. R., Sheth, H. C. & Ray, R. The feeder system of the Deccan Traps (India): insights from dike geochemistry. *J. Petrol.* **52**, 315–343 (2011).
133. Bindeman, I. et al. Pervasive hydrothermal events associated with large igneous provinces documented by the Columbia River Basaltic Province. *Sci. Rep.* **10**, 10206 (2020).
134. Park, Y., Swanson-Hysell, N. L., Lisiecki, L. E. & Macdonald, F. A. in *Large Igneous Provinces: A Driver of Global Environmental and Biotic Changes* Ch. 7 (eds Ernst, R. E., Dickson, A. J. & Bekker, A.) 153–168 (Wiley, 2021).
135. Dessert, C., Dupré, B., Gaillardet, J., François, L. M. & Allegre, C. J. Basalt weathering laws and the impact of basalt weathering on the global carbon cycle. *Chem. Geol.* **202**, 257–273 (2003).
136. Alt, J. C. & Teagle, D. A. The uptake of carbon during alteration of ocean crust. *Geochim. Cosmochim. Acta* **63**, 1527–1535 (1999).
137. Fitton, J. G. & Godard, M. Origin and evolution of magmas on the Ontong Java Plateau. *Geol. Soc.* **229**, 151–178 (2004).
138. Black, B., Mittal, T., Lingo, F., Walowski, K. & Hernandez, A. in *Large Igneous Provinces: A Driver of Global Environmental and Biotic Changes* Ch. 5 (eds Ernst, R. E., Dickson, A. J. & Bekker, A.) 117–131 (Wiley, 2021).
139. Taylor, H. P. Jr & Forester, R. W. An oxygen and hydrogen isotope study of the Skaergaard intrusion and its country rocks: a description of a 55 my old fossil hydrothermal system. *J. Petrol.* **20**, 355–419 (1979).
140. Wotzlaw, J., Bindeman, I. N., Schaltegger, U., Brooks, C. K. & Naslund, H. R. High-resolution insights into episodes of crystallization, hydrothermal alteration and remelting in the Skaergaard intrusive complex. *Earth Planet. Sci. Lett.* **355**, 199–212 (2012).
141. Mittal, T., Self, S. & Jay, A. Thickness characteristics of pāhoehoe lavas in the Deccan Province, Western Ghats, India, and in continental flood basalt provinces elsewhere. *Front. Earth Sci.* **8**, 630604 (2021).
142. Reidel, S. P., Camp, V. E., Tolan, T. L. & Martin, B. S. The Columbia River flood basalt province: stratigraphy, areal extent, volume, and physical volcanology. *Geol. Soc. Am. Spec. Pap.* **497**, 1–43 (2013).
143. Kamo, S. L. et al. Rapid eruption of Siberian flood-volcanic rocks and evidence for coincidence with the Permian–Triassic boundary and mass extinction at 251 Ma. *Earth Planet. Sci. Lett.* **214**, 75–91 (2003).
144. Blackburn, T. J. et al. Zircon U-Pb geochronology links the end-Triassic extinction with the Central Atlantic Magmatic Province. *Science* **340**, 941–945 (2013).
145. Kasbohm, J. & Schoene, B. Rapid eruption of the Columbia River flood basalt and correlation with the mid-Miocene climate optimum. *Sci. Adv.* **4**, eaat8223 (2018).
146. Kasbohm, J., Schoene, B. & Burgess, S. in *Large Igneous Provinces: A Driver of Global Environmental and Biotic Changes* Ch. 2 (eds Ernst, R. E., Dickson, A. J. & Bekker, A.) 27–82 (Wiley, 2021).
147. Burgess, S. D. & Bowring, S. A. High-precision geochronology confirms voluminous magmatism before, during, and after Earth's most severe extinction. *Sci. Adv.* **1**, e1500470 (2015).
148. Renne, P. R. et al. State shift in Deccan volcanism at the Cretaceous-Paleogene boundary, possibly induced by impact. *Science* **350**, 76–78 (2015).
149. Sprain, C. J. et al. The eruptive tempo of Deccan volcanism in relation to the Cretaceous-Paleogene boundary. *Science* **363**, 866–870 (2019).
150. Schoene, B. et al. U-Pb constraints on pulsed eruption of the Deccan Traps across the end-Cretaceous mass extinction. *Science* **363**, 862–866 (2019).
151. Ravizza, G. & Peucker-Ehrenbrink, B. Chemostratigraphic evidence of Deccan volcanism from the marine osmium isotope record. *Science* **302**, 1392–1395 (2003).
152. Dodd, S. C., Mac Niocaill, C. & Muxworthy, A. R. Long duration (>4 Ma) and steady-state volcanic activity in the early Cretaceous Paraná–Etendeka Large Igneous Province: new palaeomagnetic data from Namibia. *Earth Planet. Sci. Lett.* **414**, 16–29 (2015).
153. Schoene, B., Eddy, M. P., Keller, C. B. & Samperton, K. M. An evaluation of Deccan Traps eruption rates using geochronologic data. *Geochronology* **3**, 181–198 (2020).
154. Chenet, A., Fluteau, F., Courtillot, V., Gérard, M. & Subbarao, K. Determination of rapid Deccan eruptions across the Cretaceous-Tertiary boundary using paleomagnetic secular variation: Results from a 1200-m-thick section in the Mahabaleshwar escarpment. *J. Geophys. Res. Solid Earth* **113**, B04101 (2008).
155. Pavlov, V. E. et al. Geomagnetic secular variations at the Permian-Triassic boundary and pulsed magmatism during eruption of the Siberian Traps. *Geochem. Geophys. Geosyst.* **20**, 773–791 (2019).
156. Xu, Y., Yang, Z., Tong, Y. & Jing, X. Paleomagnetic secular variation constraints on the rapid eruption of the Emeishan continental flood basalts in southwestern China and northern Vietnam. *J. Geophys. Res. Solid Earth* **123**, 2597–2617 (2018).
157. Percival, L. M. E. et al. Mercury evidence for pulsed volcanism during the end-Triassic mass extinction. *Proc. Natl Acad. Sci. USA* **114**, 7929–7934 (2017).
158. Jones, D. S., Martini, A. M., Fike, D. A. & Kaiho, K. A volcanic trigger for the Late Ordovician mass extinction? Mercury data from south China and Laurentia. *Geology* **45**, 631–634 (2017).
159. Lindström, S. et al. Volcanic mercury and mutagenesis in land plants during the end-Triassic mass extinction. *Sci. Adv.* **5**, eaaw4018 (2019).
160. Woodruff, L. G., Schulz, K. J., Nicholson, S. W. & Dicken, C. L. Mineral deposits of the Mesoproterozoic Midcontinent Rift System in the Lake Superior region-A space and time classification. *Ore Geol. Rev.* **126**, 103716 (2020).
161. Leitch, A. & Davies, G. Mantle plumes and flood basalts: enhanced melting from plume ascent and an eclogite component. *J. Geophys. Res.* **106**, 2047–2059 (2001).
162. Jiang, Q., Jourdan, F., Olierook, H. K., Merle, R. E. & Whittaker, J. M. Longest continuously erupting large igneous province driven by plume-ridge interaction. *Geology* **49**, 206–210 (2020).
163. Mahoney, J. J., Storey, M., Duncan, R. A., Spencer, K. J. & Pringle, M. in *The Mesozoic Pacific: Geology, Tectonics, and Volcanism* Vol. 77 (eds Pringle, M. S., Sager, W. W., Sliter, W. V. & Stein, S.) 233–261 (Wiley, 1993).
164. Zhu, D. et al. The 132 Ma Comei-Bunbury large igneous province: remnants identified in present-day southeastern Tibet and southwestern Australia. *Geology* **37**, 583–586 (2009).
165. Yu, X., Lee, C. A., Chen, L. & Zeng, G. Magmatic recharge in continental flood basalts: insights from the Chifeng igneous province in Inner Mongolia. *Geochem. Geophys. Geosyst.* **16**, 2082–2096 (2015).
166. Heinonen, J. S., Luttinen, A. V., Spera, F. J. & Bohrson, W. A. Deep open storage and shallow closed transport system for a continental flood basalt sequence revealed with Magma Chamber Simulator. *Contrib. Mineral. Petrol.* **174**, 87 (2019).
167. Schmidt, A. et al. Selective environmental stress from sulphur emitted by continental flood basalt eruptions. *Nat. Geosci.* **9**, 77–82 (2015).
168. Black, B. A. et al. Systemic swings in end-Permian climate from Siberian Traps carbon and sulfur outgassing. *Nat. Geosci.* **11**, 949–954 (2018).
169. Thordarson, T. & Self, S. The Roza Member, Columbia River Basalt Group: a gigantic pahoehoe lava flow field formed by endogenous processes? *J. Geophys. Res. Solid Earth* **103**, 27411–27445 (1998).
170. Fendley, I. M. et al. Constraints on the volume and rate of Deccan Traps flood basalt eruptions using a combination of high-resolution terrestrial mercury records and geochemical box models. *Earth Planet. Sci. Lett.* **524**, 115721 (2019).
171. Petcovic, H. L. & Dufek, J. D. Modeling magma flow and cooling in dikes: implications for emplacement of Columbia River flood basalts. *J. Geophys. Res. Solid Earth* **110**, B10201 (2005).
172. Karlstrom, L., Murray, K. E. & Reiners, P. W. Bayesian Markov-Chain Monte Carlo inversion of low-temperature thermochronology around two 8–10 m wide Columbia River flood basalt dikes. *Front. Earth Sci.* **7**, 90 (2019).
173. Biasi, J. & Karlstrom, L. Timescales of magma transport in the Columbia River flood basalts, determined by paleomagnetic data. *Earth Planet. Sci. Lett.* **576**, 117169 (2021).
174. Ghosh, P., Sayeed, M., Islam, R. & Hundekari, S. Inter-basaltic clay (bole bed) horizons from Deccan traps of India: implications for palaeo-weathering and palaeo-climate during Deccan volcanism. *Palaeogeogr. Palaeoclimatol. Palaeoecol.* **242**, 90–109 (2006).
175. Olsen, P. E., Kent, D. V., Cornet, B., Witte, W. K. & Schlische, R. W. High-resolution stratigraphy of the Newark rift basin (early Mesozoic, eastern North America). *Geol. Soc. Am. Bull.* **108**, 40–77 (1996).
176. Schaller, M. F., Wright, J. D. & Kent, D. V. Atmospheric PCO_2 perturbations associated with the Central Atlantic Magmatic Province. *Science* **331**, 1404–1409 (2011).
177. Sharma, M. in *Large Igneous Provinces: Continental, Oceanic, and Planetary Flood Volcanism* (eds Mahoney, J. J. & Coffin, M. F.) 273–296 (1997).

178. Sawlan, M. G. Alteration, mass analysis, and magmatic compositions of the Sentinel Bluffs Member, Columbia River flood basalt province. *Geosphere* **14**, 286–303 (2018).
179. Xu, J., Suzuki, K., Xu, Y., Mei, H. & Li, J. Os, Pb, and Nd isotope geochemistry of the Permian Emeishan continental flood basalts: insights into the source of a large igneous province. *Geochim. Cosmochim. Acta* **71**, 2104–2119 (2007).
180. Fedorenko, V. A. & Czamanske, G. K. Results of new field and geochemical studies of the volcanic and intrusive rocks of the Maymecha-Kotuy area, Siberian flood-basalt province, Russia. *Int. Geol. Rev.* **39**, 479–531 (1997).
181. Sheth, H. C., Pande, K. & Bhutani, R. ^{40}Ar-^{39}Ar ages of Bombay trachytes: evidence for a Palaeocene phase of Deccan volcanism. *Geophys. Res. Lett.* **28**, 3513–3516 (2001).
182. Moore, N., Grunder, A. & Bohrson, W. The three-stage petrochemical evolution of the Steens Basalt (southeast Oregon, USA) compared to large igneous provinces and layered mafic intrusions. *Geosphere* **14**, 2505–2532 (2018).
183. Bennett, E. N., Lissenberg, C. J. & Cashman, K. V. The significance of plagioclase textures in mid-ocean ridge basalt (Gakkel Ridge, Arctic Ocean). *Contrib. Mineral. Petrol.* **174**, 1–22 (2019).
184. Reidel, S. P. et al. The Grande Ronde Basalt, Columbia River Basalt Group; Stratigraphic descriptions and correlations in Washington, Oregon, and Idaho. *Geol. Soc. Am. Spec. Pap.* **239**, 21–53 (1989).
185. Durand, S. R. & Sen, G. Preeruption history of the Grande Ronde formation lavas, Columbia River basalt group, American northwest: evidence from phenocrysts. *Geology* **32**, 293–296 (2004).
186. Ramos, F. C., Wolff, J. A. & Tollstrup, D. L. Sr isotope disequilibrium in Columbia River flood basalts: evidence for rapid shallow-level open-system processes. *Geology* **33**, 457–460 (2005).
187. Borges, M. R., Sen, G., Hart, G. L., Wolff, J. A. & Chandrasekharam, D. Plagioclase as recorder of magma chamber processes in the Deccan Traps: Sr-isotope zoning and implications for Deccan eruptive event. *J. Asian Earth Sci.* **84**, 95–101 (2014).
188. Bryan, S. E. et al. The largest volcanic eruptions on Earth. *Earth Sci. Rev.* **102**, 207–229 (2010).
189. Streck, M. J., Ferns, M. L. & McIntosh, W. Large, persistent rhyolitic magma reservoirs above Columbia River Basalt storage sites: the Dinner Creek Tuff eruptive center, eastern Oregon. *Geosphere* **11**, 226–235 (2015).
190. Rocha, B. C. et al. Rapid eruption of silicic magmas from the Paraná magmatic province (Brazil) did not trigger the Valanginian event. *Geology* **48**, 1174–1178 (2020).
191. Basu, A. R. et al. Widespread silicic and alkaline magmatism synchronous with the Deccan Traps flood basalts, India. *Earth Planet. Sci. Lett.* **552**, 116616 (2020).
192. Peate, D. W. Global dispersal of Pb by large-volume silicic eruptions in the Paraná-Etendeka large igneous province. *Geology* **37**, 1071–1074 (2009).
193. Cather, S. M., Dunbar, N. W., McDowell, F. W., McIntosh, W. C. & Scholle, P. A. Climate forcing by iron fertilization from repeated ignimbrite eruptions: the icehouse–silicic large igneous province (SLIP) hypothesis. *Geosphere* **5**, 315–324 (2009).
194. Tabazadeh, A. & Turco, R. P. Stratospheric chlorine injection by volcanic-eruptions: HCl scavenging and implications for ozone. *Science* **260**, 1082–1086 (1993).
195. Glaze, L., Self, S., Schmidt, A. & Hunter, S. Assessing eruption column height in ancient flood basalt eruptions. *Earth Planet. Sci. Lett.* **457**, 263–270 (2014).
196. Thordarson, T. & Self, S. The Laki (Skaftár Fires) and Grímsvötn eruptions in 1783–1785. *Bull. Volcanol.* **55**, 233–263 (1993).
197. Thordarson, T., Larsen, G., Steinthorsson, S. & Self, S. The 1783–1785 AD Laki-Grímsvötn eruptions II: Appraisal based on contemporary accounts. *Jökull* **53**, 11–47 (2003).
198. Hon, K., Kauahikaua, J., Denlinger, R. & Mackay, K. Emplacement and inflation of pahoehoe sheet flows: observations and measurements of active lava flows on Kilauea Volcano, Hawaii. *Geol. Soc. Am. Bull.* **106**, 351–370 (1994).
199. Swanson, D. A., Wright, T., Hooper, P. & Bentley, R. Revisions in stratigraphic nomenclature of the Columbia River Basalt Group (USGS, 1979).
200. Brown, R. J., Blake, S., Thordarson, T. & Self, S. Pyroclastic edifices record vigorous lava fountains during the emplacement of a flood basalt flow field, Roza Member, Columbia River Basalt Province, USA. *Geol. Soc. Am. Bull.* **126**, 875–891 (2014).
201. Jones, T. J. & Llewellin, E. W. Convective tipping point initiates localization of basaltic fissure eruptions. *Earth Planet. Sci. Lett.* **553**, 116637 (2021).
202. Wei, Z., Qin, Z. & Suckale, J. Magma mixing during conduit flow is reflected in melt-inclusion data from persistently degassing volcanoes. *ESSOAr* https://doi.org/10.1002/essoar.10505766.1 (2021).
203. Burgisser, A., Bergantz, G. W. & Breidenthal, R. E. Addressing complexity in laboratory experiments: the scaling of dilute multiphase flows in magmatic systems. *J. Volcanol. Geotherm. Res.* **141**, 245–265 (2005).
204. Witt, T., Walter, T. R., Müller, D., Guðmundsson, M. T. & Schöpa, A. The relationship between lava fountaining and vent morphology for the 2014–2015 Holuhraun eruption, Iceland, analyzed by video monitoring and topographic mapping. *Front. Earth Sci.* **6**, 235 (2018).
205. Ross, P. S. et al. Mafic volcaniclastic deposits in flood basalt provinces: a review. *J. Volcanol. Geotherm. Res.* **145**, 281–314 (2005).
206. Thordarson, T. Accretionary-lapilli-bearing pyroclastic rocks at ODP Leg 192 Site 1184: a record of subaerial phreatomagmatic eruptions on the Ontong Java Plateau. *Geol. Soc.* **229**, 275–306 (2004).
207. Pyle, D. & Mather, T. Halogens in igneous processes and their fluxes to the atmosphere and oceans from volcanic activity: a review. *Chem. Geol.* **263**, 110–121 (2009).
208. Dasgupta, R. & Hirschmann, M. M. The deep carbon cycle and melting in Earth's interior. *Earth Planet. Sci. Lett.* **298**, 1–13 (2010).
209. Wieser, P. E., Jenner, F., Edmonds, M., Maclennan, J. & Kunz, B. E. Chalcophile elements track the fate of sulfur at Kīlauea Volcano, Hawai'i. *Geochim. Cosmochim. Acta* **282**, 245–275 (2020).
210. Guex, J. et al. Thermal erosion of cratonic lithosphere as a potential trigger for mass-extinction. *Sci. Rep.* **6**, 23168 (2016).
211. Broadley, M. W., Barry, P. H., Ballentine, C. J., Taylor, L. A. & Burgess, R. End-Permian extinction amplified by plume-induced release of recycled lithospheric volatiles. *Nat. Geosci.* **11**, 682–687 (2018).
212. Gales, E., Black, B. & Elkins-Tanton, L. T. Carbonatites as a record of the carbon isotope composition of large igneous province outgassing. *Earth Planet. Sci. Lett.* **535**, 116076 (2020).
213. Liu, J. et al. Plume-driven recratonization of deep continental lithospheric mantle. *Nature* **592**, 732–736 (2021).
214. Howarth, G. H. et al. Superplume metasomatism: evidence from Siberian mantle xenoliths. *Lithos* **184**, 209–224 (2014).
215. Ernst, R. E., Davies, D. R., Jowitt, S. M. & Campbell, I. When do mantle plumes destroy diamonds? *Earth Planet. Sci. Lett.* **502**, 244–252 (2018).
216. Svensen, H. et al. Siberian gas venting and the end-Permian environmental crisis. *Earth Planet. Sci. Lett.* **277**, 490–500 (2009).
217. Aarnes, I., Svensen, H., Polteau, S. & Planke, S. Contact metamorphic devolatilization of shales in the Karoo Basin, South Africa, and the effects of multiple sill intrusions. *Chem. Geol.* **281**, 181–194 (2011).
218. Capriolo, M. et al. Deep CO_2 in the end-Triassic Central Atlantic Magmatic Province. *Nat. Commun.* **11**, 1670 (2020).
219. Hernandez Nava, A. et al. Reconciling early deccan traps CO_2 outgassing and pre-KPB global climate. *Proc. Natl Acad. Sci. USA* **118**, e2007797118 (2021).
220. Hartley, M. E., Maclennan, J., Edmonds, M. & Thordarson, T. Reconstructing the deep CO_2 degassing behaviour of large basaltic fissure eruptions. *Earth Planet. Sci. Lett.* **393**, 120–131 (2014).
221. Moore, L. R. et al. Bubbles matter: an assessment of the contribution of vapor bubbles to melt inclusion volatile budgets. *Am. Mineral.* **100**, 806–823 (2015).
222. Rosenthal, A., Hauri, E. & Hirschmann, M. Experimental determination of C, F, and H partitioning between mantle minerals and carbonated basalt, CO_2/Ba and CO_2/Nb systematics of partial melting, and the CO_2 contents of basaltic source regions. *Earth Planet. Sci. Lett.* **412**, 77–87 (2015).
223. Workman, R. K., Hauri, E., Hart, S. R., Wang, J. & Blusztajn, J. Volatile and trace elements in basaltic glasses from Samoa: implications for water distribution in the mantle. *Earth Planet. Sci. Lett.* **241**, 932–951 (2006).
224. Cabato, J. A., Stefano, C. J. & Mukasa, S. B. Volatile concentrations in olivine-hosted melt inclusions from the Columbia River flood basalts and associated lavas of the Oregon Plateau: implications for magma genesis. *Chem. Geol.* **392**, 59–73 (2015).
225. Ivanov, A. V. et al. Volatile concentrations in olivine-hosted melt inclusions from meimechite and melanephelinite lavas of the Siberian Traps Large Igneous Province: evidence for flux-related high-Ti, high-Mg magmatism. *Chem. Geol.* **483**, 442–462 (2018).
226. Blake, S., Self, S., Sharma, K. & Sephton, S. Sulfur release from the Columbia River Basalts and other flood lava eruptions constrained by a model of sulfide saturation. *Earth Planet. Sci. Lett.* **299**, 328–338 (2010).
227. Caricchi, L., Sheldrake, T. E. & Blundy, J. Modulation of magmatic processes by CO_2 flushing. *Earth Planet. Sci. Lett.* **491**, 160–171 (2018).
228. Black, B. A. & Manga, M. The eruptibility of magmas at Tharsis and Syrtis Major on Mars. *J. Geophys. Res. Planets* **121**, 944–964 (2016).
229. Burton, M. R., Sawyer, G. M. & Granieri, D. Deep carbon emissions from volcanoes. *Rev. Mineral. Geochem.* **75**, 323–354 (2013).
230. Ilyinskaya, E. et al. Globally significant CO_2 emissions from Katla, a subglacial volcano in Iceland. *Geophys. Res. Lett.* **45**, 10–332 (2018).
231. McKay, D. I. A., Tyrrell, T., Wilson, P. A. & Foster, G. L. Estimating the impact of the cryptic degassing of Large Igneous Provinces: a mid-Miocene case-study. *Earth Planet. Sci. Lett.* **403**, 254–262 (2014).
232. Gaillard, F., Scaillet, B., Pichavant, M. & Iacono-Marziano, G. The redox geodynamics linking basalts and their mantle sources through space and time. *Chem. Geol.* **418**, 217–233 (2015).
233. Jugo, P. J. Sulfur content at sulfide saturation in oxidized magmas. *Geology* **37**, 415–418 (2009).
234. Zintwana, M. P., Cawthorn, R. G., Ashwal, L. D., Roelofse, F. & Cronwright, H. Mercury in the Bushveld complex, South Africa, and the Skaergaard intrusion, Greenland. *Chem. Geol.* **320**, 147–155 (2012).
235. Le Vaillant, M., Barnes, S. J., Mungall, J. E. & Mungall, E. L. Role of degassing of the Noril'sk nickel deposits in the Permian–Triassic mass extinction event. *Proc. Natl Acad. Sci. USA* **114**, 2485–2490 (2017).
236. Macdonald, F. & Wordsworth, R. Initiation of Snowball Earth with volcanic sulfur aerosol emissions. *Geophys. Res. Lett.* **44**, 1938–1946 (2017).
237. Caricchi, L., Townsend, M., Rivalta, E. & Namiki, A. The build-up and triggers of volcanic eruptions. *Nat. Rev. Earth Environ.* **2**, 458–476 (2021).
238. Mittal, T. & Richards, M. A. The magmatic architecture of continental flood basalts II: A new conceptual model. *ESSOAr* https://doi.org/10.1002/essoar.10506092.1 (2021).
239. Chenet, A. et al. Determination of rapid Deccan eruptions across the Cretaceous-Tertiary boundary using paleomagnetic secular variation: 2. Constraints from analysis of eight new sections and synthesis for a 3500-m-thick composite section. *J. Geophys. Res. Solid Earth* **114**, B06103 (2009).
240. Braunger, S. et al. Do carbonatites and alkaline rocks reflect variable redox conditions in their upper mantle source? *Earth Planet. Sci. Lett.* **533**, 116041 (2020).
241. Reichow, M. K. et al. The timing and extent of the eruption of the Siberian Traps large igneous province: implications for the end-Permian environmental crisis. *Earth Planet. Sci. Lett.* **277**, 9–20 (2009).
242. Nielsen, T. F. The shape and volume of the Skaergaard intrusion, Greenland: implications for mass balance and bulk composition. *J. Petrol.* **45**, 507–530 (2004).
243. Bürgmann, R. & Dresen, G. Rheology of the lower crust and upper mantle: evidence from rock mechanics, geodesy, and field observations. *Annu. Rev. Earth Planet. Sci.* **36**, 531–567 (2008).
244. Caprarelli, G. & Reidel, S. P. Physical evolution of Grande Ronde Basalt magmas, Columbia River Basalt Group, north-western USA. *Mineral. Petrol.* **80**, 1–25 (2004).
245. Caprarelli, G. & Reidel, S. P. A clinopyroxene–basalt geothermobarometry perspective of Columbia Plateau (NW-USA) Miocene magmatism. *Terra Nova* **17**, 265–277 (2005).
246. Hartley, M. & Thordarson, T. Melt segregations in a Columbia River Basalt lava flow: a possible mechanism for the formation of highly evolved mafic magmas. *Lithos* **112**, 434–446 (2009).
247. Tao, Y., Putirka, K., Hu, R. & Li, C. The magma plumbing system of the Emeishan large igneous province and its

role in basaltic magma differentiation in a continental setting. *Am. Mineral.* **100**, 2509–2517 (2015).
248. Putirka, K. D. Thermometers and barometers for volcanic systems. *Rev. Mineral. Geochem.* **69**, 61–120 (2008).
249. Black, B. A., Elkins-Tanton, L. T., Rowe, M. C. & Peate, I. U. Magnitude and consequences of volatile release from the Siberian Traps. *Earth Planet. Sci. Lett.* **317–318**, 363–373 (2012).
250. Liu, Z. et al. Unusually thickened crust beneath the Emeishan large igneous province detected by virtual deep seismic sounding. *Tectonophysics* **721**, 387–394 (2017).
251. Cherepanova, Y., Artemieva, I. M., Thybo, H. & Chemia, Z. Crustal structure of the Siberian craton and the West Siberian basin: an appraisal of existing seismic data. *Tectonophysics* **609**, 154–183 (2013).
252. Wolff, J. et al. Source materials for the main phase of the Columbia River Basalt Group: geochemical evidence and implications for magma storage and transport. *Geol. Soc. Am. Spec. Pap.* **497**, 273–291 (2013).
253. Barry, T. et al. Eruption chronology of the Columbia River Basalt Group. *Geol. Soc. Am.* **497**, 45–66 (2013).
254. Thordarson, T. & Höskuldsson, Á. Postglacial volcanism in Iceland. *Jökull* **58**, e228 (2008).
255. Neal, C. A. et al. The 2018 rift eruption and summit collapse of Kīlauea Volcano. *Science* **363**, 367–374 (2019).
256. Lipman, P. W. & Calvert, A. T. Modeling volcano growth on the Island of Hawaii: deep-water perspectives. *Geosphere* **9**, 1348–1383 (2013).
257. Storey, M., Duncan, R. A. & Tegner, C. Timing and duration of volcanism in the North Atlantic Igneous Province: implications for geodynamics and links to the Iceland hotspot. *Chem. Geol.* **241**, 264–281 (2007).
258. Matthews, S., Shorttle, O., Rudge, J. F. & Maclennan, J. Constraining mantle carbon: CO_2-trace element systematics in basalts and the roles of magma mixing and degassing. *Earth Planet. Sci. Lett.* **480**, 1–14 (2017).
259. Self, S., Widdowson, M., Thordarson, T. & Jay, A. E. Volatile fluxes during flood basalt eruptions and potential effects on the global environment: a Deccan perspective. *Earth Planet. Sci. Lett.* **248**, 518–532 (2006).
260. Callegaro, S. et al. Microanalyses link sulfur from large igneous provinces and Mesozoic mass extinctions. *Geology* **42**, 895–898 (2014).
261. Saal, A. E., Hauri, E. H., Langmuir, C. H. & Perfit, M. R. Vapour undersaturation in primitive mid-ocean-ridge basalt and the volatile content of Earth's upper mantle. *Nature* **419**, 451–455 (2002).
262. Sibik, S., Edmonds, M., Maclennan, J. & Svensen, H. Magmas erupted during the main pulse of Siberian Traps volcanism were volatile-poor. *J. Petrol.* **56**, 2089–2116 (2015).
263. Sobolev, A., Krivolutskaya, N. & Kuzmin, D. Petrology of the parental melts and mantle sources of Siberian trap magmatism. *Petrology* **17**, 253–286 (2009).
264. Black, B. A., Hauri, E. H., Elkins-Tanton, L. T. & Brown, S. M. Sulfur isotopic evidence for sources of volatiles in Siberian Traps magmas. *Earth Planet. Sci. Lett.* **394**, 58–69 (2014).
265. Self, S., Blake, S., Sharma, K., Widdowson, M. & Sephton, S. Sulfur and chlorine in late Cretaceous Deccan magmas and eruptive gas release. *Science* **319**, 1654–1657 (2008).
266. Choudhary, B. R., Santosh, M., De Vivo, B., Jadhav, G. & Babu, E. Melt inclusion evidence for mantle heterogeneity and magma degassing in the Deccan large Igneous Province, India. *Lithos* **346**, 105135 (2019).
267. Davis, K. N., Wolff, J. A., Rowe, M. C. & Neill, O. K. Sulfur release from main-phase Columbia River Basalt eruptions. *Geology* **45**, 1043–1046 (2017).
268. Zhang, Y., Ren, Z. & Xu, Y. Sulfur in olivine-hosted melt inclusions from the Emeishan picrites: implications for S degassing and its impact on environment. *J. Geophys. Res. Solid Earth* **118**, 4063–4070 (2013).
269. Marks, L. et al. F, Cl, and S concentrations in olivine-hosted melt inclusions from mafic dikes in NW Namibia and implications for the environmental impact of the Paraná–Etendeka Large Igneous Province. *Earth Planet. Sci. Lett.* **392**, 39–49 (2014).
270. Peate, D. W., Peate, I. U., Rowe, M. C., Thompson, J. M. & Kerr, A. C. Petrogenesis of high-MgO lavas of the Lower Mull Plateau Group, Scotland: insights from melt inclusions. *J. Petrol.* **53**, 1867–1886 (2012).
271. Thordarson, T., Self, S., Oskarsson, N. & Hulsebosch, T. Sulfur, chlorine, and fluorine degassing and atmospheric loading by the 1783–1784 AD Laki (Skaftár Fires) eruption in Iceland. *Bull. Volcanol.* **58**, 205–225 (1996).
272. Clarkson, M. O. et al. Ocean acidification and the Permo-Triassic mass extinction. *Science* **348**, 229–232 (2015).

Acknowledgements
T.A.M. acknowledges funding from ERC consolidator grant (ERC-2018-COG-818717-V-ECHO). B.A.B. acknowledges funding from NSF EAR 1615147. L.K. acknowledges funding from NSF EAR 1848554.

Author contributions
All authors participated in drafting and revising the article. B.A.B. and T.A.M. led the discussion of volatiles and created the volatile compilation, L.K. led the discussion of formation-level and member-level tempo, B.A.B. and L.K. led the discussion of the structure of large igneous provinces and their relationship to other volcanic activity, B.A.B. led the discussion of mantle melt generation.

Competing interests
The authors declare no competing interests.

Peer review information
Nature Reviews Earth & Environment thanks R. Ernst, L. Kirstein and B. Schoene, and the other, anonymous, reviewer(s) for their contribution to the peer review of this work.

Publisher's note
Springer Nature remains neutral with regard to jurisdictional claims in published maps and institutional affiliations.

Supplementary information
The online version contains supplementary material available at https://doi.org/10.1038/s43017-021-00221-4.